Stabilisation of Tyrosine Hydroxylase in Nanoparticles for Enzyme Replacement Therapy

Maria Teresa Bezem

This thesis is submitted in partial fulfilment of the requirements for the degree of Master of Science as part of the work during the Master's programme in Nanoscience.

Department of Biomedicine

University of Bergen

February 2012

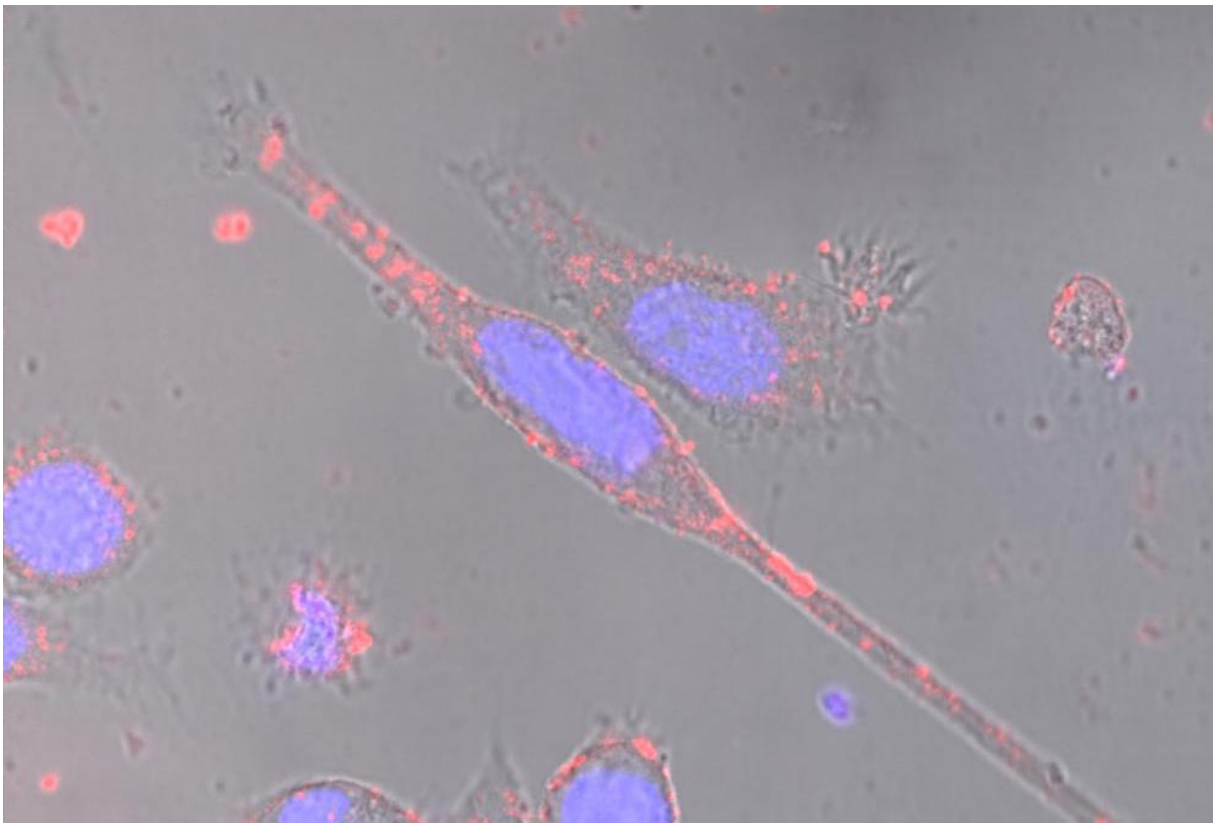

Abstract

The aim of this thesis has been to characterise nanoparticles (NPs) to which tyrosine hydroxylase (TH) was attached, as a preliminary step in their evaluation to be used for an enzyme replacement therapy (ERT) for Parkinson's disease (PD). TH is the enzyme catalysing the rate-limiting step in the synthesis of catecholamines, an important group of neurotransmitters. It converts dietary L-tyrosine to L-3,4-dihydroxyphenylalanine (L-DOPA). Levels of dopamine, one of the catecholamines, are low in the brain of patients with PD. Typical treatment is the supply of L-DOPA, at least short-term it improves the patient's quality of life, but also gives side effects and motor impairment after many years of use. A transport of TH to the brain is expected to naturally increase the amount of L-DOPA and dopamine if L-tyrosine and the cofactor tetrahydrobiopterin are present. This was the envisioned ERT in this project. The NPs were selected based on their ability to absorb large amounts of protein, to cross an *in vitro* model of the blood-brain barrier and because they consist mainly of cross-linked maltodextrin, a biodegradable polymer. TH used in this study was recombinant human enzyme, and we found that expression of TH in a fusion protein with a ZZ-carrier as a partner protein, provided a homogeneous, active enzyme at high yield. The binding between TH and the NPs was investigated by atomic force microscopy, size determination using dynamic light scattering and size exclusion chromotography. The changes in enzymatic activity of TH during a 24 hours time-lapse, were measured by an assay using radioactively labelled tyrosine, and the uptake of NP-bound TH into cells was evaluated by confocal microscopy. TH was found to be absorbed into the pores of the NPs upon titration with increasing concentration of TH, which showed a small but steady increase in the size of the NPs, as well as a phase change upon atomic force microscopy visualisation. TH's enzymatic activity was initially reduced by the NPs, but on the long run stabilised by them, and even further stabilisation was obtained in the presence of oxidative protecting enzymes or when inhibited by dopamine. Confocal imaging of TH with a fluorescent label, showed that all four different cell types that were tested, could take up TH only when it was bound to NPs. These results show the potential of these NPs to deliver TH and their potential application for ERT.

Front figure: PC12 cells were incubated with Alexa Fluor 568 labelled tyrosine hydroxylase (red) and of which the nuclei had been stained with 4,6-diamindino-2-phenylindole (blue) before imaging with Leica TCS SP5, a confocal microscope.

Oppsumering

Målet med denne masteroppgaven har vært å karakterisere nanopartikler som tyrosin hydroksylase har blitt bundet til, for å kunne evaluere om de kunne brukes til en enzymerstatningsterapi for Parkinson's sykdom. Tyrosin hydroxylase er et enzym som katalyserer den hastighetsbestemmende reaksjonen i syntesen av katekolaminene som er en viktig gruppe innenfor nevrotransmittere. Det katalyserer L-tyrosin fra kosten til L-3,4-dihydroksyfenylalanin. Nivået av dopamin, en av katekolaminene, er lavt i hjernen til Parkinsons pasienter. Typisk behandling er tilførsel av L-3,4-dihydroksyfenylalanin, som ved siden av en positiv innvirking på pasientenes liv, også har bivirkninger og gir problemer med motorikken etter langvarig bruk. Ved å transportere tyrosin hydroksylase til hjernen, kan nivået av både L-3,4-dihydroksyfenylalanin og dopamin økes på en naturlig måte, dersom kofaktoren tetrahydrobiopterin og L-tyrosin er tilstede. Dette var i sikte da ideen om enzymerstatningsterapi ble utarbeidet. Nanopartiklene ble valgt ut ifra deres egenskap til å kunne absorbere store mengder protein, krysse en *in vitro* model av blod-hjerne barrieren og fordi de er laget av polymerisert maltodekstrin som er bionedbrytbart. Bindingen mellom tyrosin hydroksylase og nanopartiklene ble studert ved hjelp av atomkraftmikroskop og størrelsesmålinger med dynamisk lysspredning og gelfiltreringskromotografi. Endringene i enzymaktiviteten til tyrosin hydroksylase over en 24 timers periode ble målt med radioaktiv stråling, og opptaket av nanopartikkelbundet tyrosin hydroksylase i celler ble evaluert i konfokalmikroskopet. Tyrosin hydroksylase var i dette prosjektet rekombinant humant enzym og vi fant ut at uttrykking av tyrosin hydroksylase som et fusjonsprotein sammen med et annet protein gav et homogent og aktiv enzym med høyest avkastning. Det ble funnet ut at nanopartiklene absorberer tyrosin hydroxylase ved observasjonen av en liten, men gjevn økning i nanopartikkelstørrelse under en konsentrasjontitrering av tyrosin hydroksylase. Tyrosin hydroksylases enzymaktivitet ble først redusert av nanopartiklene, men i det lange løpet stabilisert av dem og enda mer stabilisering ble oppnådd når enzymer som beskytter det oksidative miljøet var tilstede eller når tyrosin hydroksylase ble hemmet av dopamin. Konfokalbilder som ble tatt av fluorescerende tyrosin hydroksylase viser at all fire celletypene som ble testet kunne ta opp enzymet, men kun når det var bundet til en av nanopartiklene. Disse resultatene viser potensiale som disse nanopartiklene har til å levere tyrosin hydroksylase til hjernen og deres bruk i en enzymerstatningsterapi.

Contents

Acknowledgement

First of all I would like to express my deep gratitude to my supervisor Professor Aurora Martinez for being so inspiring and encouraging. Professor Aurora Martinez is thanked very much for introducing me to an exciting field of research and for always helping me in the interpretation of the obtained results and the design of the next experiments.

Thanks to my cosupervisor Knut Teigen for initial structural investigations, and to Didier Betbeder and his group for sending the nanoparticles and for a nice and useful stay in the lab at the Université de Lille 2 in France. I would like to thank all the biorecognizers and a special thank to Anne Baumann for teaching me TH activity and help with the AFM and the precise feedback on writing, Ana Jorge-Finnigan for teaching me cell culture and confocal microscopy and great comments on my writing and Marte Flydal for teaching me recombinant protein expression.

Furthermore, I want to thank all the other master students at the Department of Biomedicine for including me, and for all the lunch breaks we have had together. I also want to thank the other nanostudents: Tom Mordal and Oddgeir Randa and esspecially Stein-Erik Gullaksen for sharing the process of becoming a researcher in the new field of nanotechnology.

Finally I want to thank my friends and family for all their support I have received. Trine, Tina and Vigdis, you have been so flexible when I have been so busy. Gunnar, Geir Olav, Stein-Arild and Tu, you never stopped inviting me on activities and trips for which I am very happy. A special thank to Eirik Oen Lie for printing this thesis. At last, but not at least, I want to thank Yrjan, thank you for your love and encouragment.

Abbreviations

AA	amino acid
AAAH	aromatic amino acid hydroxylase
AFM	atomic force microscopy
BBB	blood-brain barrier
BH_4	tetrahydrobiopterin
DLS	dynamic light scattering
FPLC	fast protein liquid chromatography
L-DOPA	L-dihydroxyphenylalanine
MBP	maltose binding protein
NP	nanoparticle
PAH	phenylalanine hydroxylase
PCR	polymerase chain reaction
PD	Parkinson's disease
RT	room temperature
SDS-PAGE	sodium dodecyl sulfate polyacrylamide gel electrophoresis
SEC	size exclusion chromatography
TH	tyrosine hydroxylase
TPHs	tryptophan hydroxylases
UV	ultraviolet
ZZ-carrier	fusion partner containing a double synthetic Z-domain

Abbreviations of chemicals can be found in the chemical list (Section 3.6) and standard or well-known abbreviations, or those used only once, are not listed.

1 Introduction

1.1 Nanomedicine in drug delivery

Nanotechnology is used in an increasing number of areas of both industry and research. In medicine for example, nano-scaled carrier devices can be loaded with drugs to improve the pharmaceutical effect. Before nanotechnology became integrated in the development of pharmaceutics, drugs have been selected by two distinguished properties: their pharmaceutical action and their targeting abilities. Many potential drugs are rejected because they lack the ability to selectively accumulate in the organ or cell type of interest and can therefore not ensure their own delivery to the correct site. The separation of these properties into a drug substance and a carrier substance revolutionises the ideas about how to develop new treatments [1] and shows the huge potential of nanotechnology in medicine.

Nanocarriers are usually nanoparticles (NPs) that can transport the drug to a certain tissue or organ in the body like the brain [2, 3, 4, 5] and even to specific cells with an identifiable receptor on their surface. In the latter case, the nanoacarrier should contain the right antibody against its specific receptor. Nanocarriers could also include other systems, for example are nanotubes used [6]. Advances are made in sub-cellular targeting of the drug by the help of nanocarriers which directs the drug to a predetermined site within the cell [1].

Specific targeting by recognition of the nanocarrier by a receptor is in general obtained by modifying NPs at their surface. The recognition will then hopefully be proceeded by internalisation of the NP, usually by endocytosis - a process where the membrane deforms into small balls called endosomes, including the external substance at their inside. The fate of the NP will then differ according to the type of particle and its surface modifications.

1.2 Medication to the brain - the blood-brain barrier (BBB)

The brain is the most important organ in our body and is therefore well protected. It has its own immune system and the ways in and out, through which nutrients and other

physiological important molecules flow, are tightly regulated. Only few pharmaceutics are therefore able to treat the brain. Several membranes separate the brain from the rest of the body. One of them is the blood-brain barrier (BBB) which has to be crossed by medicaments in order to enter the brain. There also exist different administration routes for drugs targeting the brain like the nasal pathway. Hitherto the BBB seems the most effective way for delivery of drugs to the brain [7]. Almost all neurons in the brain are in contact with a capillary blood vessel. The effectiveness is also reflected in the huge surface area of the BBB compared to the other barriers.

1.2.1 Physiology of the BBB

The BBB consists of a membrane of both blood vessel cells and brain cells, usually of the type called astrocytes (Figure 1.1). A layer of tightly packed endothelial cells make up the blood vessel wall of all the small capillaries nourishing the brain. The structure of these capillaries differs from those in the rest of the body by not having an inter-cellular passage between the cells. The cells make up a nice layer by having tight junctions almost gluing them together. The side of the endothelial cells that does not face the blood is approximately 96% covered with end-feet from mainly astrocytes. Astrocytes are glial cells situated between neurons also called nerve cells, in the brain [8]. In contrast to neurons, they do not conduct any nerve signal.

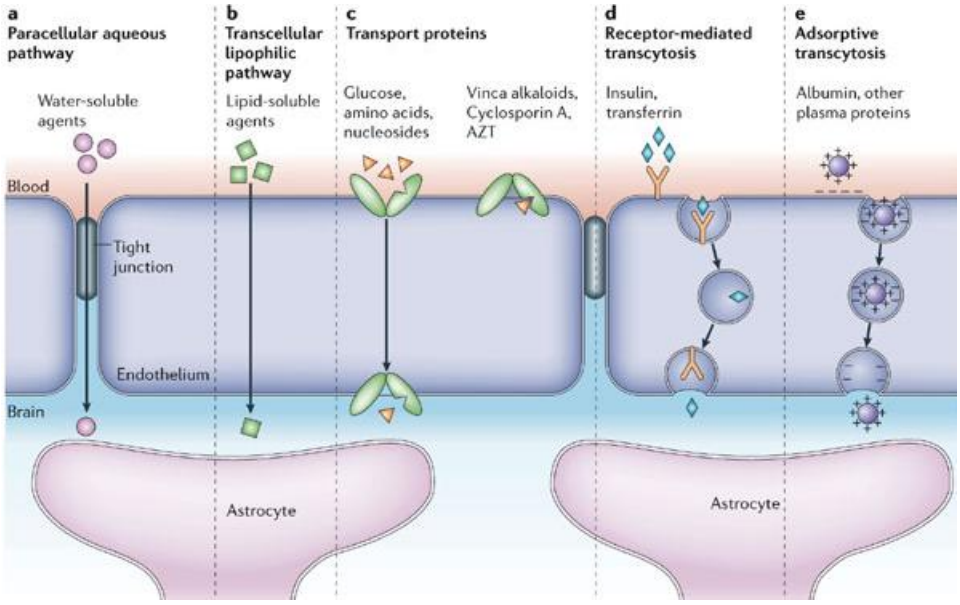

Figure 1.1: The blood-brain barrier and mechanisms for transport across it. Reprinted with permission from Macmillan Publishers Ltd: Nature Reviews Neuroscience [9], copyright (2006).

1.2.2 Nanoparticles for transport across the BBB

The transport in and out of the brain is heavily controlled [7]. Six different transport mechanisms across the BBB are known: passive diffusion and the five pathways illustrated in figure 1.1. The nanocarriers are most likely to be transported by either the receptor-mediated or the adsorptive transcytosis [10, 11]. The big size of the nanocarriers prevents it from using passive diffusion which usually only works for small hydrophobic molecules. The para-cellular aqueous pathway and the trans-cellular lipophilic pathway are reserved for hydrophilic or hydrophobic molecules, respectively, whereas transport proteins can only be used by specific molecules like nutrients and signal molecules.

The typical administration route to the brain is through the blood before crossing the BBB. The phagocytes, a type of white blood cell, could easily degrade the foreign NPs in the blood. This process is facilitated by opsonisation which is the binding of opsonine proteins that mark the NPs for this preliminary degradation [12]. NPs must therefore be designed in order not to be recognised by opsonins.

Another issue to address is the toxicology of the NPs. NPs for use in treatments should be biodegradable and not toxic to the patient. The degradation of the NPs after they have performed their pharmaceutical action, must be ensured to avoid undesired effects. Many NPs are therefore made of biologically degradable polymers like the well-studied polylactide-co-glycolide (PLGA) or the less known gelatin, chitosan or maltodextrin [13]. It is therefore easy for the body to take all parts from each other and degrade each substance by itself.

1.3 Parkinson's disease

Parkinson's disease (PD) is characterized by cell-death in a part of the middle brain called substantia nigra. Neurons in this brain area are responsible for the biosynthesis of dopamine, and their specific death results in a decrease of dopamine levels. Since dopamine is a crucial neurotransmitter for the circuit of information flow for motoric abilities, a progressive movement disorder including the well-known tremor is characteristic of PD [8].

The typical treatment of PD is symptomatic and aims at increasing the dopamine levels by oral supply of dopamine through the dopamine precursor L-3,4-dihydroxyphenylalanine (L-DOPA) [14]. The overall effect of the treatment is positive, as patients experience an improved quality of life and a reduced mortality rate. L-DOPA remains therefore the standard to which all new treatments are compared [15].

On the long run there are side effects and lower responsiveness to L-DOPA. Long term use of levodopa implies the development of motor complications and alternative treatments are therefore investigated. Cell transplants and gene therapy focus more on the delivery of dopamine in a more physiological manner [16]. The alternative treatment envisioned in this master's project, is the use of enzyme replacement therapy to deliver the enzyme tyrosine hydroxylase to the brain for the biosynthesis of dopamine.

1.4 The tyrosine hydroxylase enzyme system

1.4.1 Tyrosine hydroxylase

Tyrosine hydroxylase (TH) is an important enzyme only expressed in a few organs. It catalyses the conversion of the amino acid L-tyrosine to L-DOPA (Figure 1.2) which can be further metabolised to the catecholamines dopamine, noradrenaline and adrenaline. The catecholamines are an important group of neurotransmitters in the central nervous system. Neurotransmitters are molecules that transfer an electrical signal coming along the axon of neurons to a chemical signal. They cross the synaptical cleft, which is a small space between two neurons, to transfer the signal. In this way the next neuron can receive and carry on the signal along its own axons. TH is the enzyme catalysing the rate limiting step in the catecholamine biosynthesis (Figure 1.2).

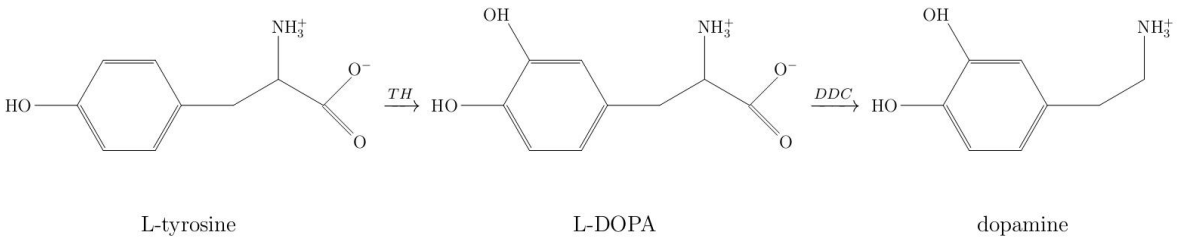

Figure 1.2: The biosynthesis of dopamine. The first step converses dietary L-tyrosine to L-3,4-dihydroxyphenylalanine (L-DOPA) and is catalysed by tyrosine hydroxylase (TH). The second step converses L-DOPA to dopamine and is catalysed by DOPA decarboxylase (DDC).

1.4.2 Aromatic amino acid hydroxylase family

TH, phenylalanine hydroxylase (PAH) and the tryptophan hydroxylases (TPH1 and TPH2) are all part of the aromatic amino acid hydroxylase (AAAH) family. They are similar in both primary structure (Figure 1.3), quaternary structure (Figure 1.4) and function.

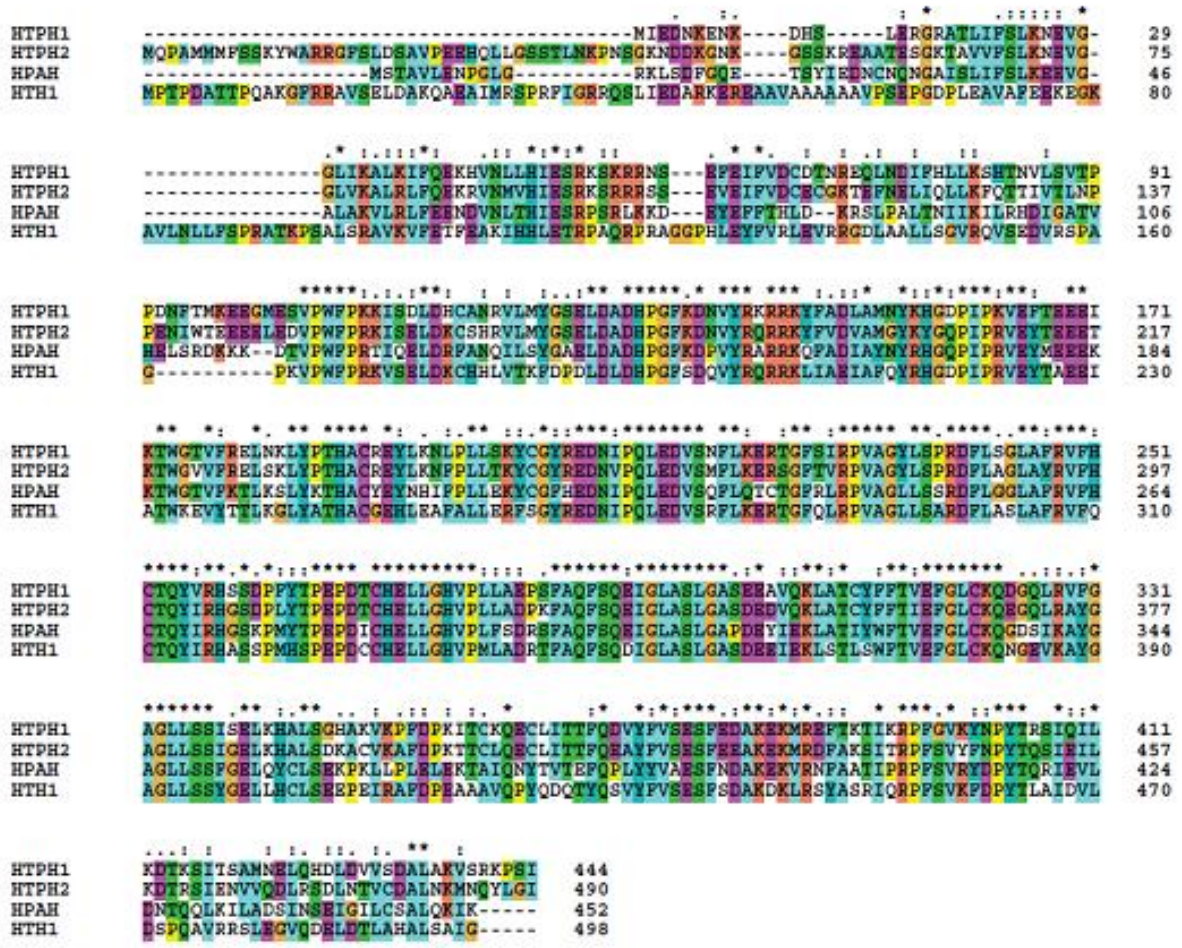

Figure 1.3: Sequence alignment of the aromatic amino acid hydroxylases (AAAHs) human tryptophan hydroxylase 1 and 2 (HTPH1 and HTPH2), human phenylalanine hydroxylase (HPAH) and human tyrosine hydroxylase 1 (HTH1) [17]. The asterisks above the sequence indicate identical amino acids at this position and the dots indicate the degree of similarity between the amino acid sequences of the AAAHs.

The monomers, which are the subunits of the enzymes, consist of three domains: first the regulatory domain at the amino terminus, in the middle the catalytic domain and at last the polymerisation domain at the carboxyl-terminus (Figure 1.4). X-ray diffraction derived crystal structures are known for the latter two domains, whereas the amino terminal's regulatory domain is flexible and has so far failed to crystallise. The monomers are very similar in primary structure, that is the amino acid sequence, especially at the catalytic domain where the amino acid substrate binds to become hydroxylated. As in TPH1 and TPH2 human TH is a homotetramer (Figure 1.4), containing four identical subunits and so are the TPHs, whereas PAH can be a dimer or tetramer.

Each AAAH catalyses the incorporation of an -OH group on an aromatic amino acid

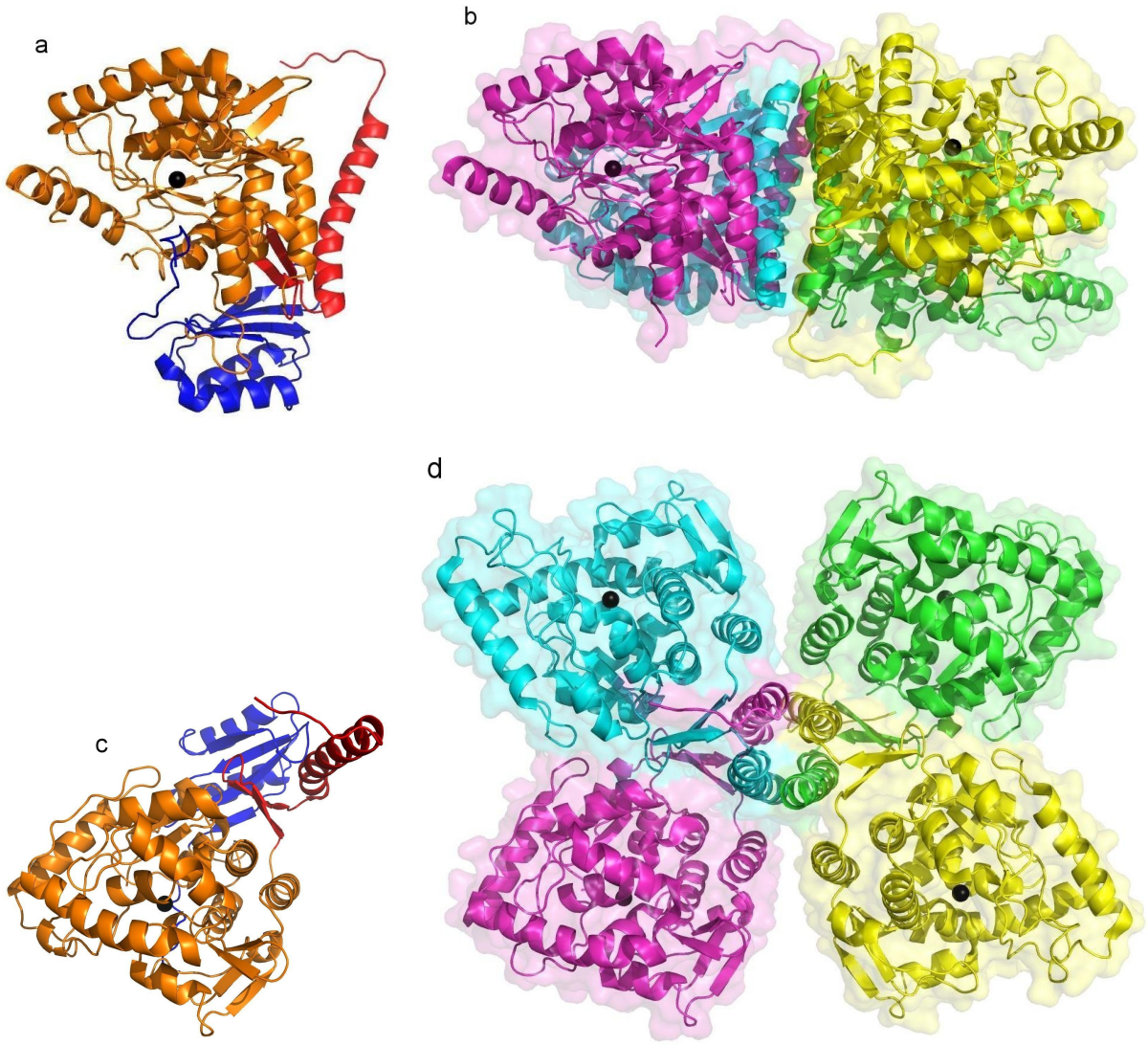

Figure 1.4: Cartoon representations of the structure human tyrosine hydroxylase where the iron in each subunit is shown as a black sphere. The crystal structure is determined by X-ray crystallography and found in the protein data bank (PDB). (a) Side view of a monomer where the amino terminus regulatory domain (blue) is derived from crystal structures of human TH (PDB-ID 2XSN; non published results) and the catalytic domain (orange) and the oligomerisation domain (red) containing the carboxyl terminus is derived from rat PAH (PDB-ID 2phm; [18]). (b) Side view of the tetrameric structure of the biological assembly of TH with each monomer in its own colour (PDB-ID 2xsn). This structure is similar to the structure from the rat enzyme (PDB-ID 1TOH; [19]). (c) Top view of the monomer. (d) Top view of the tetramer. The monomers are oriented the same way as the pink subunit of the tetramer. The images were generated by PyMOL (Schrödinger).

using molecular oxygen and the cofactor tetrahydrobiopterin (BH_4) (Figure 1.5).

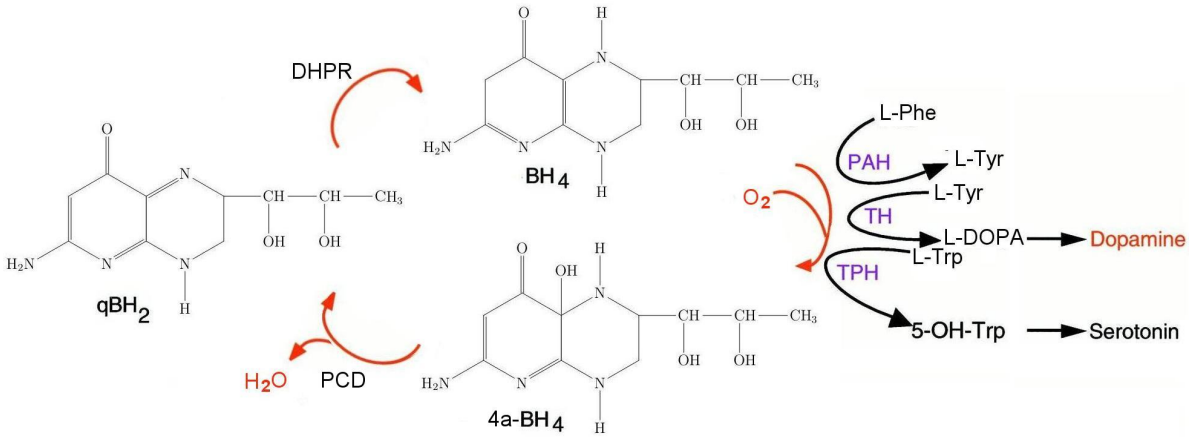

Figure 1.5: The mechanism for the aromatic amino acid hydroxylases including the regeneration of the cofactor tetrahydrobiopterin (BH_4). 4 a$-BH_4$ = BH_4-4a-carbinolamine; 5-OH-Trp = 5-hydroxytryptophan; DHBR = dihydropteridine reductase; L-Phe = L-phenylalanine; L-Trp = tryptophan; L-Tyr = L-tyrosine; PCD = pterin-4a-carbinolamine dehydratase; qBH_2 = quinoid-dihydrobiopterin. Figure modified from [20] and [21].

1.4.3 The cofactor tetrahydrobiopterin

BH_4 is the cofactor for all the AAAHs. It is converted to tetrahydrobiopterin-4a-carbinolamine (4a-BH4) and further to quinoid-dihydrobiopterin (qBH2) during the reaction catalysed by TH (Figure 1.5). BH_4 competes with the catecholamines which bind to the active site and inhibit the enzymatic activity of TH. This end product inhibition will regulate the production of catecholamines in synergy with cyclic adenosine mono phosphate (AMP)-dependent phosphorylation, a modification that releases the catecholamine inhibition [22]. No further biosynthesis is needed when there are high concentrations of dopamine and other final catecholamine products that then will bind and inhibit TH.

1.4.4 The non-heme iron II ion

Each TH-monomer coordinates an iron II ion (Fe^{2+}) at the catalytic site. The iron is coordinated by three amino acid residues and one to three water molecules [23]. The iron must be protected from oxidation, as it is easily converted to catalytically inactive Fe^{3+}. Antioxidants and enzymes responsible for the redox balanced environment of the cell can therefore stabilise TH and preserve the enzymatic activity by ensuring the right oxidation state of iron, like is known for PAH [24].

1.4.5 Inherent instability

TH is a protein that is difficult to work with in the lab. It has an inherent instability, as its catalytic activity is easily inactivated and it readily aggregates [25]. Aggregates are large complexes of macromolecules that can no longer be kept in solution, aggregation is a non-reversible reaction that *in vivo* can result in cell death. TH is sensitive to the contents of the solution it is dissolved in, as it needs a relatively crowded and redox balanced environment to avoid its tendency to aggregate.

1.4.6 Enzyme replacement therapy

Enzyme replacement therapy (ERT) is a strategy to deliver the enzyme in its functional form to the site where it is needed to carry out its activity. This therapeutic approach is being increasingly used for the treatment of genetic disorders like the rare Fabry disease [26] or Gaucher disease [27]. We have envisioned that such a therapy could be developed with TH for Parkinson's disease and this is the final aim of the work carried out in this Master's thesis. The ERT with TH might also be useful for related diseases where a mutation in the gene for TH causes a TH deficiency [28].

1.5 Purpose

It is expected that the levels of dopamine will increase when providing TH in its functional form to the brain. This assumes that the substrate L-tyrosine and the cofactor BH_4 are already present. The goal of this master project is to contribute to the development of an ERT for PD or related diseases which uses catalytic NPs showing high enzymatic activity and stability. The main objective of this work is to obtain functionalised NPs with TH bound, that are able to enter cells. The NPs NP^+ and $DPPGNP^+$ will be evaluated for their potential as carriers of TH by investigation of their characteristics.

Another important purpose of this work is both to gain competence in the different experimental methods that can be used to study proteins and/or NPs and to acquire knowledge about the well-established scientific field of TH and the use of NPs in medical research.

1.5.1 Specific aims

Three subprojects have been defined with the following specific aims:

1. To probe the binding between the NPs and TH.
2. To evaluate the changes in TH activity upon binding.
3. To investigate if the NPs can deliver TH to cells.

1.5.2 Choice of methods

The first aim will be addressed by using dynamic light scattering (DLS) and atomic force microscopy (AFM) to determine the size and surface structure respectively, complemented with size exclusion chromatography (SEC). Enzyme activity is measured by a radioactive assay with tritium-labelled tyrosine to see if TH preserves its function upon binding to the NPs as stated in the second aim. The last aim will require cell culture experiments and imaging with confocal microscopy.

1.5.3 Hypotheses

The NPs that will be used in the work of this master's thesis are known to be porous and positively charged [29] and are therefore expected to bind the slightly negatively charged TH, at neutral pH TH's isoelectric point (pI) is 6.11. The binding is hypothesised to rely on weak intermolecular interactions and based on previous studies on the binding of TH to liposomes it is expected that the enzyme will bind through the regulatory domain [30], so that the catalytic activity will be maintained.

However, TH could loose its enzymatic activity if its conformation is altered too much. Since there is no covalent bond expected between the NP and TH, the conformation is expected to be only slightly modified upon binding.

The selected NPs are shown to deliver other proteins successfully to cells [31]. TH is therefore also expected to be delivered.

2 Theoretical and methodological considerations

2.1 Theoretical considerations

2.1.1 Tyrosine hydroxylase

TH is similar in sequence of amino acids (AAs), the protein's primary structure to both PAH and the TPHs as they all are part of the AAAH enzyme family (Figure 1.3). The sequence identity is greater than 80% in the catalytic domain [32]. The crystal structure for the sequence from amino acid 193 and to the carboxyl terminus is known for the human TH (Figure 1.4). The amino-terminus is mobile and the structure is not known yet.

TH that I have worked with is splicing isoform 1 (SWISS-PROT ID P07101) and is presented in the sequence alignment (Figure 1.3). The AAs 31 to 61 are missing compared to isoform 3 due to alternative splicing (not shown). The total length is therefore 497 AAs and the molecular weight 55 612 Da. The theoretical diameter can be calculated by measuring the longest distance in the crystal structure that is known (Figure 1.4d). When this is done in Discovery (Accelerys), the calculated diameter is 11.9 nm. The regulatory domain at the amino terminus is for PAH located on top of the tetramer [18] and this can reasonable be expected for TH as well. The diameter will therefore not increase by the presence of the regulatory domain, but just give the structure a more spherical appearance instead of a slightly flat square.

2.1.2 The nanoparticle system

There are two types of NPs (Figure 2.1) that have been selected for the work presented in this thesis [29]. They are called NP^+ and $DPPGNP^+$. Both consist mainly of maltodextrin - an oligomer of glucose and is thus a sugar compound which can easily be degraded biologically. During the synthesis the maltodextrin is cross linked giving a polysaccharide and porous particle [33]. The particles are positively charged due to the incorporation of the cationic ligand glycidyltrimethylammonium (GTMA) which can aid protein absorption. $DPPGNP^+$ are in addition functionalised with dipalmitoylphosphatidylglycerol

(DPPG) which is a lipid giving more rigidity to the structure as it is expected to fill the core of the porous particles.

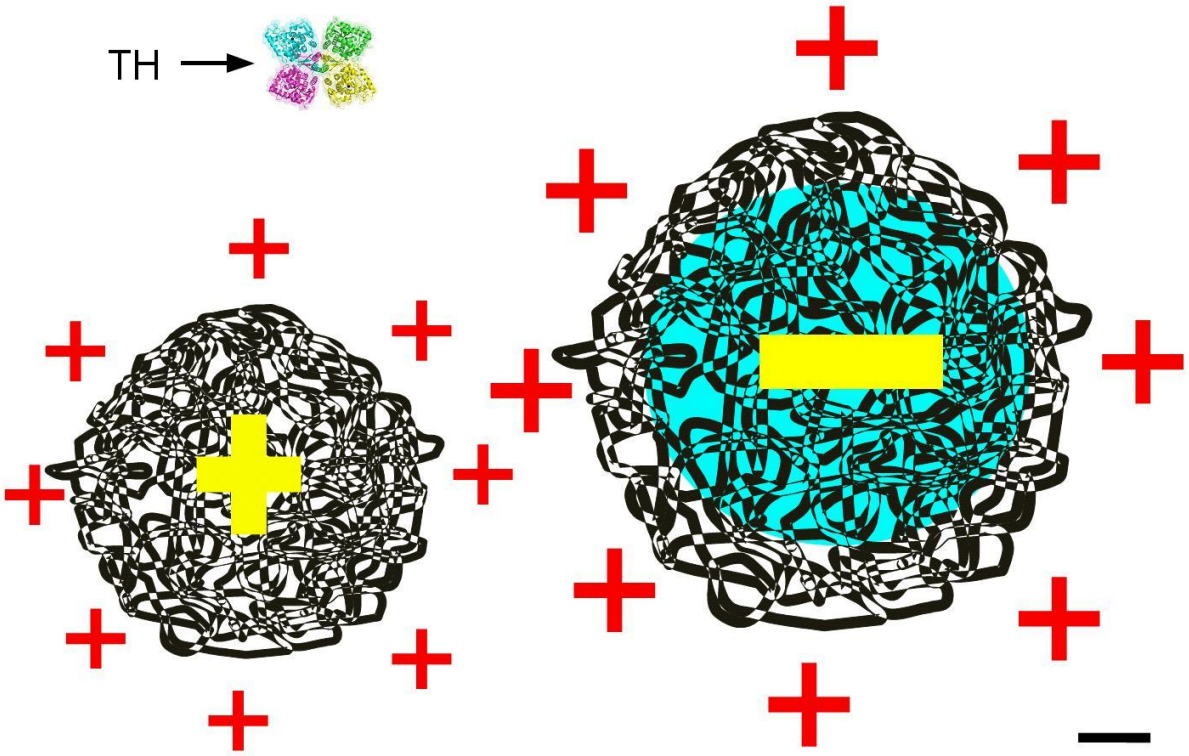

Figure 2.1: The nanoparticles NP^+ (left) and DPPGNP+ (right). The maltodextrin polymer gives the porous structure (black and white), whereas the positive surface charge (red) is due to the GTMA. The inner charge (yellow) of GTMA is cancelled out by the lipid core of DPPG (blue) for the biggest particle. TH is shown to scale (many colours) and the scale bar is 10 nm.

The NPs behave as sponges and absorb high amounts of protein or lipid [29]. If assuming spherical shape for TH, there will be 25 THs per NP if the weight to weight ratio is 1:1. Nanoparticles, when present in the blood, are often quickly detected by opsonins which are proteins that mark a foreign substance so that it can be degraded. By loading and saturating the cationic NPs with negatively charged sustances like the protein of interest, in this case TH, the opsonation is inhibited and the NPs have a longer circulation time in the blood [29].

It has also been observed that NP^+ are transcytosed across a cellular model of the BBB, whereas the same experiment for $DGGPNP^+$ was inconclusive due to difficulties in the procedure [34]. These NPs seem therefore a suitable choice to be tested as a nanocarrier of TH for ERT in Parkinson's disease and related malignancies.

It is important to know the NPs toxicology because if the NPs are to be used for human administration, then they should not impair a danger on the patient. The toxicology of

NP^+ has been studied in detail, showing no apparent damage on cells or on DNA except at very high doses [35] which would not occur *in vivo*.

2.2 Methodological considerations

Here I will only present the non-typical methods that have been used. Please continue to the methods chapter for the details on the standard biochemical methods as recombinant protein expression and purification, gel electrophoresis and chromatography.

2.2.1 Dynamic light scattering

DLS is a method for size determination of small particles in suspension in the nanometre range, including proteins. A monochromatic laser light is shown through the solution containing the suspended particles and the refracted laser light intensity pattern is recorded at a certain angle (Figure 2.2). The pattern changes over time according to rate of diffusion of particles in solution. Small particles will move fast and give a fast changing intensity pattern, whereas larger particles will diffuse slower through the medium and give a less changing intensity pattern. The intensity patterns are compared over time giving a correlation function (Figure 2.2). The rate of diffusion is determined by the correlation function.

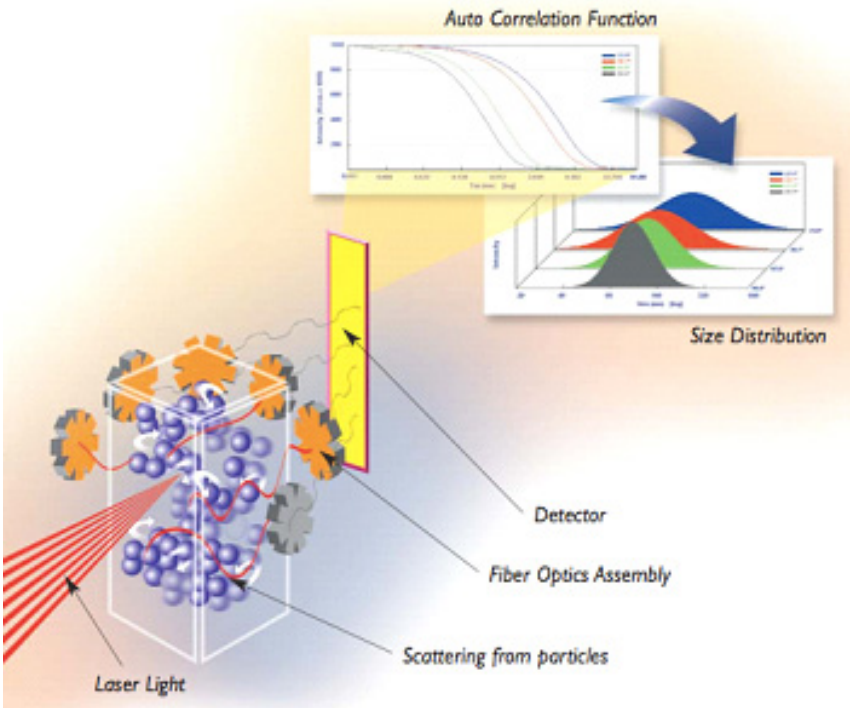

Figure 2.2: The principle of dynamic light scattering [36].

The particles' radius can then be calculated by the Einstein-Stokes relation (equation 2.1) where D: rate of diffusion, T: temperature, η: viscosity of solution and R: particle radius.

$$D = \frac{kT}{6\pi\eta R} \tag{2.1}$$

DLS works well for particles that easily scatter the laser beam, meaning that their refractive index is different from the medium in which they are suspended. In addition the particles are assumed to refract the beam indifferent of their orientation which means that they have to be spherical, so for non-spherical particles the radius will be less exact. Another challenge is that samples should be a homogeneous suspension and no sedimentation should occur during the measurement. The movement will then not be random diffusion and no longer only depend on the size. In addition, the sample should be uniformly distributed, containing only particles of the same size as it is not possible to distinguish between types of particles by DLS. Neither should the samples contain aggregates, dust or other contaminations as big particles of course scatter the laser beam much more efficiently than small particles, giving an unnatural proportion of big versus small particles.

2.2.2 Atomic force microscopy

AFM is a high resolution imaging method where a cantilever with a small tip scans over the sample surface and is deflected by the intermolecular forces. There exist different modes depending if the tip is in the range of repulsive forces that dominate in the closest region above the surface or in the range of attractive forces (Figure 2.3a). Tapping mode makes the cantilever arm vibrate so that both regions are covered. While the cantilever scans over the surface and is deflected up and down according to the surface structure and composition, the laser beam will be reflected with a smaller and bigger angle according to the deflection. The changes in the laser beam reflection angle are detected by a photo diode for each position of the cantilever tip (Figure 2.3b). In this way the result for each point is visualised as one pixel.

AFM images show three different modes of the same picture: Height, amplitude and phase. The height image mode represents the sample surface's topography. The imaging was done in tapping mode, therefore the tip vibrates at a specific frequency. These vibrations have an amplitude and phase, just like all other waves, which change according to the forces exerted on the tip by the sample surface. The amplitude and the phase retrace show the variations in the amplitude and phase of the tip vibration, respectively.

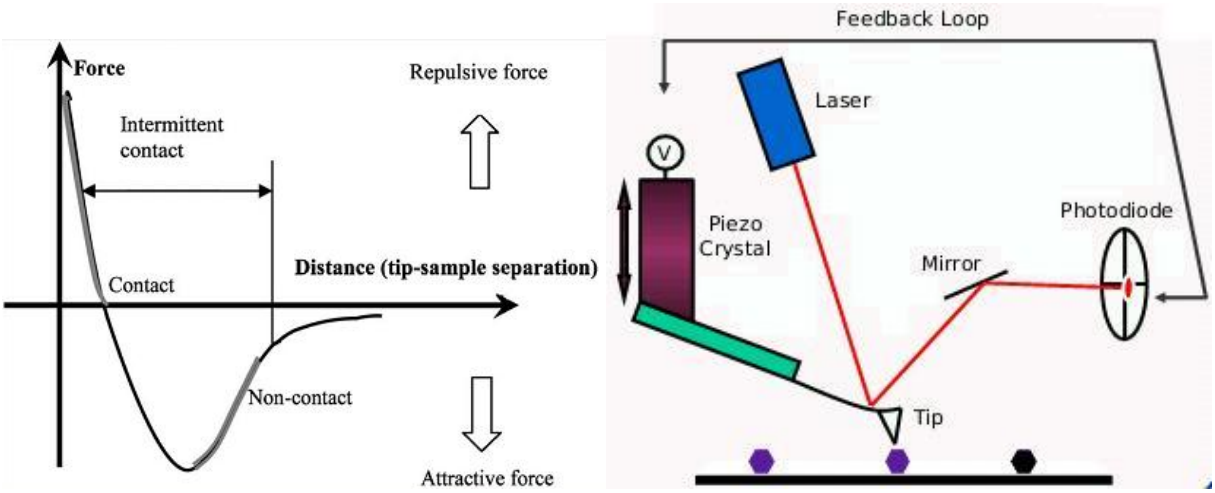

Figure 2.3: The principle of atomic force microscopy. (a) The force between the tip and the sample surface changes with the distance between them [37]. (b) The laser light is deflected when the cantilever arm is deflected due to a change in the force between the tip and the sample surface [38].

AFM works very fine for inorganic samples with a hard surface. Changes in the surface's structure or composition can then be seen in either of the images. Sometimes the AFM's high resolution is also needed for biological samples having a soft surface. The imaging procedure is then much more difficult as the cantilever tip can scrape into the sample surface or parts of the sample can stick to the tip and be moved around interfering with the scanning.

AFM devices can be grouped in two categories, one for imaging and one for force measurements between tip and sample. The AFM instrument that has been used for the work presented in this thesis is best suited for force measurements. The quality of the images taken is therefore not the best.

2.2.3 Confocal microscopy

Confocal microscopy is a combination of old fashioned light microscopy where the light is focussed onto the sample and fluorescence microscopy where the sample is fluorescent. Fluorescence is a property of certain chemical substances that have the ability to emit light with high intensity at a specific wavelength when excited by light of a shorter wavelength. To obtain a high resolution, the laser light is focussed as a spot onto the sample which then illuminates only a small part of the sample. The spot is then scanned over the sample surface to give an image of the whole sample. At each point some parts of the sample will get excited and emit light of a lower wavelength, e.g. when green laser light is used for excitation, red light is emitted (Figure 2.4). The emitted light is detected, recorded

and shown on a computer screen.

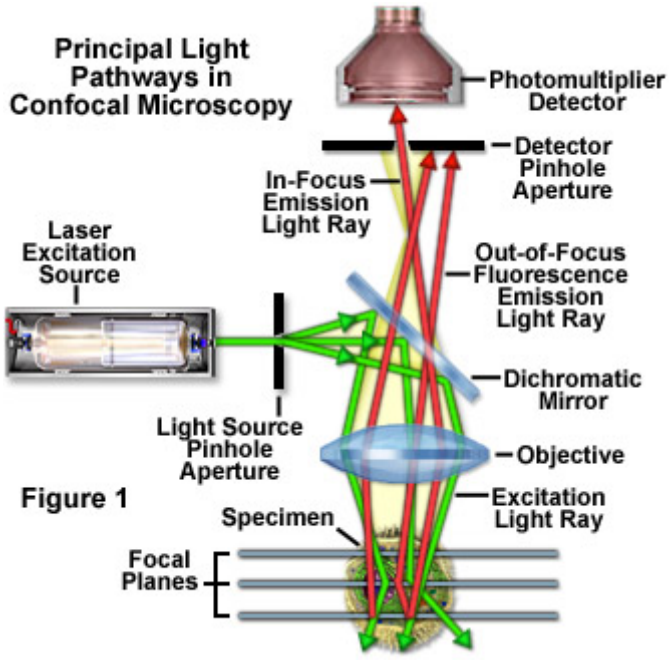

Figure 2.4: The principle of confocal microscopy [39].

Usually several laser lights are used to excite each their specific fluorescent substance in the sample. Resolution for a 63x oil immersion objective with numerical aperture 1.4 is 0.24 μm for green light. Oil immersion is to avoid a refraction and therefore loss of info at the interface of two media. Since objectives with a high numerical aperture due to their high magnification have a very limited depth of field, the sample is easily moved out of focus. 3-D pictures can be obtained by moving the sample through the focal plane of the lenses.

Resolution is still limited by diffraction of the light waves which again depends on the wavelength. To increase the resolution, the wavelength has to be shortened, which for example is obtained when using electrons instead of UV or visible light as done in electron microscopy. Another challenge is that the sample needs to be fluorescent. Not all features in a sample can become fluorescent although this can both be obtained by covalent binding to a fluorescent dye by the use of fluorescent antibodies or through fusion to a fluorescent protein.

2.2.4 Tyrosine hydroxylase activity assay

The TH enzymatic activity was measured by a radioactive assay using tritated tyrosine, for details see methods section 4.6. To ensure the availability of BH_4 and to avoid the

accumulation of its oxidised forms, BH_4 is kept reduced by the presence of the reducing agent dithiothreitol (DTT) in the assay. DTT in this way substitutes the enzymes that *in vivo* catalyse the steps back to the reduced form of BH_4 (Figure 1.5) [21] .

The experiments were only performed in two parallels because the timing is crucial for the assay's accuracy and reproducibility. Proper statistics for each experiment could therefore not be performed because the standard deviation is calculated from only two parallels. However, experiments were performed several times at slightly different conditions, so the trends that the graphs presented show, are representative.

Before starting the work with radioactivity, I took the internal training course of the University of Bergen in radiation protection and use of ionising radiation.

3 Materials

3.1 Instruments

Method	Instrument	Provider
Atomic force microscopy	Molecular force probe 3D	Asylum Research
Concentration measurements	Nanodrop ND-1000	Saveen Werner
Centrifugation	Centrifuge 5810R	Eppendorf
Dynamic light scattering	Nanosizer Z	Malvern Nordic
Cell culture (incubator)	Heraeus Hera Cell 150	Tamro Medlab
Bacteria culture	Excella E24 Incubator Shaker	New Brunswick Scientific
Liquid scintillation analyzer	Tri-carb 2900TR	Packard
Size exclusion chromatography	Biologic duoflow	BioRad-Laboratories

3.2 Nanoparticles

Name	Provider
Nanoparticles of maltodextrin (NP^+)	D. Betbeder (gift)
Nanoparticles of maltodextrin and dipalmitoylphosphatidylglycerol ($DPPGNP^+$)	D. Betbeder (gift)
Fluorescent $DPPGNP^+$ which are labelled with dioctadecyl tetramethylindocarbocyanine perchlorate (DiI))	D. Betbeder (gift)
Gold nanoparticles coated with MUA (Au-MUA)	Wilhelm Glomm (gift)

3.3 Enzymes

Name	Provider
Acc651	New England Biolabs
AmpliTaq Gold	Applied Biosystems
Catalase bovine liver, lyophilized powder	Sigma Aldrich
Nco1	New England Biolabs
Restriction protease factor Xa	Boehringer-Mannheim
Superoxide dismutase (SOD) from bovine erythrocytes	Sigma Aldrich
Taq DNA polymerase	England Biolabs Inc.
Tobacco etch virus (TEV) protease	Günther Stier (gift)
T4 DNA ligase	Fermentas

3.4 Cell lines and bacteria

Name	Provider
16HBE14o- (human bronchial epithelial cell line)	Customary cell line in the lab of D. Betbeder
Escherichia coli strain BL21-CodonPlus(DE3)RIL	Stratagene
Escherichia coli XL10-Gold ultracompetent cells	Stratagene
HEK293 (human embryonic kidney cell line)	Eystein Oveland (gift)
NCI-H292 (human epithelial cell line)	Customary cell line in the lab of D. Betbeder
PC12 (cell line derived from rat pheochromocytoma)	Originally a gift from Stein Ove Døskeland, now a customary cell line at Aurora Martinez's lab

3.5 Medium and cell equipment

Name	Provider
4-well plates	Nunc
8-well Lab-Tek chamber slides	Thermo Scientific
Bovine serum	Sigma Aldrich
Dulbecco's modified Eagle's medium (DMEM)	Sigma Aldrich
Fetal bovine serum (FBS)	Sigma Aldrich
Horse serum	Invitrogen
Prolong Gold with DAPI antifading reagent	Life technologies
Roswell Park Memorial Institute (RPMI) medium	Sigma Aldrich

3.6 Chemicals

Name	Provider
4',6-diamidino-2-phenylindole (DAPI)	Invitrogen
4-(2-hydroxyethyl)-1-piperazineethanesulfonic acid (HEPES)	Sigma Aldrich
Acetic acid (CH_3COOH)	Sigma Aldrich
Adenosine 3'-5'-cyclic monophosphate	Sigma Aldrich
Agar-agar	Merck
Agarose	Sigma Aldrich
α-lactose	Sigma Aldrich
Ammonium iron (II) sulphate hexahydrate ($(NH_4)_2Fe(SO_4)_2 \cdot H_2O$)	Sigma Aldrich
Ammonium sulfate ($(NH_4)_2SO_4$)	Sigma Aldrich

Name	Provider
Blue dextran	Sigma Aldrich
Bromophenol Blue	Merck
Charcoal activated	Merck
Compound III (3-amino-2-benzyl-7-nitro-4-(2-quinolyl)-1,2-dihydroisoquinolin-1-one)	Maybridge Ltd.
Coomassie brilliant blue R-250	Bio-Rad
Cytochrom c	Sigma Aldrich
Deoxynucleotriphosphates mix, 10 mM (dNTPs)	Invitrogen
Distilled water	Milli-Q
Dimethyl sulfoxide (DMSO)	Sigma Aldrich
Dopamine	Sigma Aldrich
Dithiothreitol (DTT)	Sigma Aldrich
Ethanol	Sigma Aldrich
Ethylenediaminetetraacetic acid (EDTA)	Sigma Aldrich
Fluorescein isothiocyanate (FITC)	Sigma Aldrich
GelRed Nucleic Acid Stain	Biotium
Glutamine (Gln)	Sigma Aldrich
Glycerol	Merck
Glucose	Sigma Aldrich
Hydrogen chloride (HCl)	VWR International
Imidazole	Sigma Aldrich
Isopropanol	Sigma Aldrich
Isopropyl thiogalactoside (IPTG)	Sigma Aldrich
LSC-cocktail Emulsifier-safe	PerkinElmer
L-[3,5-^{3}H]-tyrosine (tritium-labelled)	GE Healthcare
L-Tyrosine	Sigma Aldrich
Kanamycin	Sigma Aldrich
Magnesium dichloride ($MgCl_2$)	Applied Biosystems
Magnesium sulfate ($MgSO_4$)	Sigma Aldrich
Paraformaldehyde (PFA)	Fluka
Pefabloc SC PLUS	Roche
Penicilin	Invitrogen
Penicilin and streptomycin mix, 100 x	Sigma Aldrich
Pepstatin A, microbial	Sigma Aldrich
Peptone from casein, pancreatic digest	Sigma Aldrich
Phenylmethanesulfonylfluoride (PMSF)	Sigma Aldrich
Phosphate buffer saline tablets	Sigma Aldrich
Poly-L-lysine	Roche
Potassium chloride (KCl)	VWR International
Potassium phosphate monobasic (KH_2PO_4)	VWR International
PSC-Protector solution	Roche
Sodium bicarbonate ($NaHCO_3$)	Sigma Aldrich
Sodium carbonate (Na_2CO_3)	Sigma Aldrich
Sodium chloride (NaCl)	Sigma Aldrich

Name	Provider
Sodium dodecyl sulfate (SDS)	Sigma Aldrich
Sodium phosphate dibasic dihydrate ($Na_2HPO_4 \cdot 2\,H_2O$)	Sigma Aldrich
Streptomycin	Invitrogen
Tetrahydrobiopterin (BH_4)	Schircks Laboratories
Trizma base primary standard and buffer (Tris-HCl)	Sigma Aldrich
Trypsin	Biochrom
Trypsin –EDTA solution	Sigma Aldrich
Tryptone	Sigma Aldrich

3.7 Other products

Product name	Provider
Alexa Fluor 568 Protein Labeling Kit	Molecular Probes
Amersham Biosciences PD-10 desalting column	GE Healthcare
GeneRuler 1 kb DNA ladder	Fermentas
HiLoad Superdex prep grade Column	GE Healthcare
NEBuffer 3 10 x	New England Biolabs
PCR Gold buffer 10 x	Applied Biosystems
pETZZ-1a plasmid	Günther Stier (gift)
PureYield TM Plamid MidiprepSystem	Promega
TALON Superflow Metal Affinity Resin	Clontech Laboratories
ThermoPol Buffer 10x	Pall Life Sciences
QIAquick gel extraction kit	Qiagen
QIA PCR purification kit	Qiagen
Yeast extract nitrogen base without amino acids	Sigma Aldrich

3.8 Buffers and solutions

3.8.1 Autoinduction medium

The autoinduction medium is made as a combination of the following mixtures:

Name	Final concentration	Chemical	Molecular weight	Amount
ZY	1.08 % (w/v)	Tryptone	–	10 g
	0.54 % (w/v)	Yeast extract	–	5 g
	–	Water	–	925 ml
NPS	0.5 M	$(NH_4)_2SO_4$	132.14 g/mol	6.6 g
	1 M	KH_2PO_4	136.09 g/mol	13.6 g
	1 M	$Na_2HPO_4 \cdot 2\,H_2O$	141.96 g/mol	17.8 g
	–	Water	–	90 ml
5052	0.5% (w/v)	Glycerol	92.09 g/mol	25 g
	0.05% (w/v)	Glucose	180.16 g/mol	2.5 g
	0.2% (w/v)	α-lactose	342.30 g/mol	10 g
	–	Water	–	73 ml
$MgSO_4$	1 M	$MgSO_4 \cdot 7\,H_2O$	246.47 g/mol	24.65 g
	–	Water	–	100 ml

5052 is heated in the microwave in order to dissolve the lactose. All the mixtures are autoclaved individually and mixed as follows:

Volume	Mixture
928 ml	ZY
50 ml	NPS
20 ml	5052
2 ml	1 M $MgSO_4$

This gives the following final concentrations:

Final concentration	Chemical
1% (w/v)	Tryptone
0.5% (w/v)	Yeast extract
0.5 M	$(NH_4)_2SO_4$
1 M	KH_2PO_4
1 M	$Na_2HPO_4 \cdot 2\,H_2O$
0.5% (w/v)	Glycerol
0.05% (w/v)	Glucose
0.2% (w/v)	α-lactose
2 mM	$MgSO_4 \cdot 7\,H_{20}$

3.8.2 Complete Dulbecco's modified Eagle's medium

Final concentration	Chemical	Initial concentration	Volume
–	DMEM	–	500 ml
10% (v/v)	FBS	100%	55 ml
2 mM	Glutamine	226 mM	5 ml
1 x	Penicilin/Streptomycin mix	100 x	5 ml

New glutamine was added every 3 weeks to prevent a lower concentration due to

spontanous deamination. In the lab of Prof. Didier Betbeder, the antibiotics were added separately with final concentration of 100 U/ml penicilin and 100 μg/ml streptomycin.

3.8.3 Complete Roswell Park Memorial Institute medium

Final concentration	Chemical	Initial concentration	Volume
–	RPMI	–	500 ml
10% (v/v)	Horse serum	100%	55 ml
10% (v/v)	Bovine serum	100%	55 ml
2 mM	Glutamine	226 mM	5 ml
1 x	Penicilin/Streptomycin mix	100 x	5 ml

New glutamine was added every 3 weeks to prevent a lower concentration due to spontanous deamination.

3.8.4 Destaining solution

Final concentration	Chemical	Initial concentration	for 1 l
30% (v/v)	EtOH	Absolute	300 ml
5% (v/v)	Acetic acid	99.8%	50 ml

3.8.5 FPLC buffer

Concentration	Chemical	Molecular weight (Mw)	for 1 l
20 mmol	HEPES	238.3 g/mol	4.77 g
200 mM	NaCl	58.44 g/mol	11.69 g

The pH is adjusted to 7.0 with 2 M NaOH before all the water is added. The buffer is filtered, degassed and cooled down to 4°C.

3.8.6 HEPES buffer

Concentration	Chemical	Mw (g/mol)	for 100 ml
400 mmol	HEPES	238.3	9.53 g

The pH is adjusted to 7.0 with 2 M NaOH before all the water is added. Half of it is diluted 1:20 with water to give a 20 mM buffer.

3.8.7 Liquid Luria-Bertani (LB) medium

Concentration	Chemical	Mw (g/mol)	for 1 l
–	Peptone	–	10 g
–	Yeast extract	–	5 g
171 mM	NaCl	58.44	10 g

After the components are mixted, LB medium is autoclaved.

3.8.8 Luria-Bertani agar plates

15 mg agar is added to a liter of liquid Luria Broth (LB) medium to obtain a 1.5% agar concentration. The mixture is autoclaved and cooled to 55°C and 20 ml is poured in each plate in a sterile environment. The plates are dried for 45 min.

3.8.9 4% (w/v) Paraformaldehyde

1 g paraformaldehyde (PFA) is dissolved in 25 ml phosphate buffered saline (PBS) by continuous stirring at 65°C and left to cool down.

3.8.10 46 mM Pefabloc solution

Concentration	Chemical	Mw (g/mol)	Amount mixed
46 mM	Pefabloc SC Plus	239.7	12.5 mg
8.8 mM	HEPES pH 7.0	238.3	500 μl
–	PSC-Protector solution	–	625 μl

3.8.11 Phosphate buffered saline (PBS)

Concentration	Chemical	Mw (g/mol)	for 1 l
140 mM	NaCl	58.44	8.18 g
2.7 mM	KCl	75.55	0.20 g
10 mM	Na_2HPO_4	177.99	1.8 g
1.8 mM	KH_2PO	136.09	0.24 g

The pH is approximately 7.4. Alternatively a phosphate buffer saline tablet is dissolved in 200 ml by magnetic stirring.

3.8.12 4 x SDS denaturation buffer

Concentration	Chemical	Mw (g/mol)	for 10 ml
250 M	Tris-HCl, pH 6.8	157.60	9.53 g
8% (w/v)	SDS	288.38	0.8 g
40% (v/v)	Glycerol	92.09	4 ml
75 mM	DTT	154.25	0.116 g
0.02%	Bromophenol Blue	669.96	0.002 g

SDS denaturation buffer is usually stored in aliquotes of 95 μl without the dithiothreitol (DTT) at -20°C. The DTT is added right before use.

3.8.13 Super optimal broth with catabolite repression (SOC) medium

Concentration	Chemical	Initial	for 1 l
2% (w/v)	Tryptone	–	20 g
0.5% (w/v)	Yeast extract	–	5 g
0.05% (w/v)	NaCl	58.44 g/mol	0.5 g
1 M	KCl	400 M stock	2.5 ml
20 mM	$MgCl_2$	1 M stock	2 ml
20 mM	Glucose	1 M stock	2 ml

All components, except the magnesium chloride and the glucose are mixed and the medium is autoclaved. Right before use magnesium chloride and glucose are added.

3.8.14 Staining solution

0.25 g Coomassie Blue is dissolved in 250 ml destaining solution and all is filtered.

3.8.15 Stop solution

Concentration	Chemical	Mw (g/mol)	for 500 ml
7.5 (w/v) %	Charcoal activated	12.01	37.5 g
1 M	HCl (aq)	36.46	500 ml

3.8.16 TAE buffer

Concentration	Chemical	Mw (g/mol)	for 1 l
40 mM	Tris-HCl	157.60	6.3 g
20 mM	Acetic acid	60.05	1.02 g
1 mM	EDTA	292.24	0.29 g

3.8.17 TALON equilibration/wash buffer

Concentration	Chemical	Mw (g/mol)	for 1 l
20 mM	$Na_2HPO_4 \cdot 2\,H_2O$	141.96	2.84 g
300 mM	NaCl	58.44	17.53 g
1 μg/ml	Pepstatin	685.89	0.001 g

3.8.18 Tank buffer

Concentration	Chemical	Mw (g/mol)	for 1 l
19 mM	Tris-HCl	157.60	3 g
0.1%	SDS	288.38	1 g
156 mM	Glycerol	92.09	14.4 g

4 Methods

4.1 Recombinant tyrosine hydroxylase (TH)

TH was purified following two different novel expression and purification strategies (to be published). For the first strategy in brief, human TH, isoform 1 (hTH1), was expressed in *Escherichia coli* (*E. coli*) as a fusion protein with maltose binding protein (MBP) which was cleaved with restriction protease factor Xa at a ratio 1:200; hTH1 was then further purified by size exclusion chromatography on a HiLoad Superdex column (1.6 cm x 60 cm; GE Healthcare). The enzyme was up-concentrated by ultrafiltration with filters with a cut-off of 30 kDa and stored in liquid nitrogen until use. This first procedure was kindly performed by Ali Javier Muñoz Sepulveda, Department of biomedicine, UiB and the obtained TH was used throughout this thesis unless otherwise stated. The second strategy was developed during this Master's work together with Marte Innselset Flydal, also from the Department of biomedicine and is described in detail below.

4.1.1 *TH* gene amplification

The *TH* gene was amplified from 45 and 90 ng DNA template which was the plasmid vector pMAl-c5x/TH1 containing the *TH-MBP* gene. The conditions were 1 x GeneAmp PCR Gold buffer (150 mM Tris-HCl, pH 8.0, 500 mM KCl), 2.5 mM $MgCl_2$, 0.2 mM deoxynucleoside triphosphates (dNTPs) and 5 U/μl Amplitaq Gold with 0.2 μM of both the forward primer (TH-pETZZ-F; 5'-GCTTCCATGGGACCCACCCCCGACGCCA-3') and the reverse primer (TH-pETZZ-R; 5'-GCTTGGTACCCAGTGCAGGACCAGGGGA-3') in a final volume of 50 μl. The primers were designed such that a Nco1 and an Acc651 restriction site (underlined) were introduced at the start and after the end of the *TH* gene, respectively. The polymerase chain reaction (PCR) steps included 2 min at 95°C, 7 x (20 sec at 95°C, 20 sec at 54°C and 2 min at 74°C) and 20 x (30 sec at 95°C, 30 sec at 68°C and 2 min at 72°C) and a final elongation of 10 min at 72°C. The size of the PCR product was evaluated by agarose gel electrophoresis as described below.

4.1.2 Cloning

The PCR products (1549 basepairs) were purified with a Qiagen Purification Kit and cut with the restriction enzymes Acc561 and Nco1. The conditions during the cutting process

were 1 x NEBuffer 3 (100 mM NaCl, 50 mM Tris-HCl, 10 mM $MgCl_2$, 1 mM DTT, pH 7.9 at 25°C), 1% (w/v) bovine serum albumin (BSA), 200 U/ml of each Acc651 and Nco1 in a total volume of 50 μl. The samples were incubated 11 hours at 37°C. Approximately 1 μg of vector pET-ZZ-1a containing a different gene between the Nco1 and the Acc651 restriction sites, was cut in the same way and separated from the 'old' insert by agarose gel electrophoresis. The vector fragment was cut out from the agarose gel and purified by a Qiagen gel extraction kit. The *TH* gene was cloned into the pET-ZZ-1a vector by T4 DNA ligase in a total volume of 20 μl including 2 μl vector fragment, 15.5 μl cut *TH* gene, 1 x T4 DNA ligase buffer (40 mM Tris-HCl, 10 mM $MgCl_2$, 10 mM DTT, 0.5 mM ATP, pH 7.8 at 25°C) and 0.0625 U/μl T4 DNA ligase. The vector pETZZ-1a/TH thus contains an open reading frame coding for the fusion protein called ZZ-TH from which TH can be cleaved at the tobacco etch virus (TEV) protease cleavage site which is situated between the fusion partner and TH in the fusion protein (Figure 4.1) [40]. The fusion partner consists of a his-tag at the amino terminus, twice a Z-domain, a synthetic IgG-binding domain based on staphylococcal protein A [41], and a TEV cleavage site. The his-tag consists of six histines useful for metal affinity chromatography during the purification steps. The fusion partner is called a ZZ-carrier because of the double synthetic Z-domain.

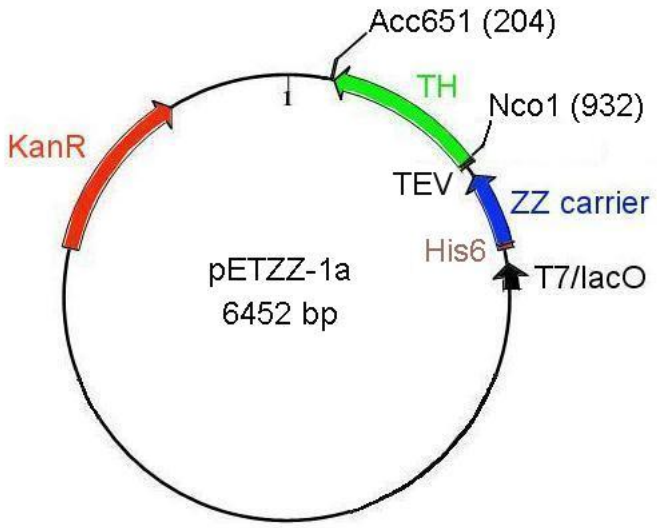

Figure 4.1: Scheme of pETZZ-1a vector with the inserted *TH* gene. Modified from [42]

4.1.3 Vector amplification

E. coli XL10-Gold ultracompetent cells (Stratagene) were transformed with the ligation mixture containing pETZZ-1a/TH vector as follows: 3 μl of the ligation was added to 37.5 μl of cells, incubated 30 min on ice, 30 sec at 42°C and 2 min on ice before 400 μl of super

optimal broth with catabolite repression (SOC) was added. The samples were incubated 45 min at 37°C and 200 rpm. 50 μl of each sample was plated on Luria-Bertani (LB) agar plates with 30 μg/ml kanamycin to select for bacteria containing pET-ZZ-1a/TH1. The LB-plates with cells were incubated upside down at 37°C overnight. Some of the colonies were screened directly for the presence of pET-ZZ-1a/hTH1 by colony PCR. In colony PCR, the bacterial colony is resuspended in a drop of medium and used as a template for the PCR-reaction. The PCR-reaction contained 1 x ThermoPol buffer (20 mM Tris-HCl, 10 mM $(NH_4)_2SO_4$, 10 mM KCl, 2 mM $MgSO_4$, 0.1% Triton X-100, pH 8.8 at 25°C), 25 U/μl Taq DNA polymerase, 0.2 mM dNTPs and 0.4 mM of each primer (TH-pETZZ-F and TH-pETZZ-R). The PCR program was initiated by 10 min at 95°C, followed by 30 x (30 sec at 95°C, 30 sec at 55°C and 2 min at 72°C) and finished by a final elongation of 2 min at 72°C. Two colonies containing amplified *TH* gene were chosen for a 50 ml culture in liquid LB medium containing 30 μg/ml kanamycin and incubated at 37 °C and 200 rpm overnight. 0.7 ml of each bacteria culture was stored in 15% (v/v) glycerol at -80°C. From the rest of the bacteria cultures, plasmids were isolated with PureYield TM Plasmid Midiprep System. The newly isolated plasmids where doublechecked for the presence of the *TH* gene by cutting them with the restriction enzymes Acc651 and Nco1 under the same conditions as previously described. The excision of the *TH* gene was verified by agarose gel electrophoresis.

4.1.4 Expression of recombinant TH in *Echerichia coli* cells

Two 50 μl of *E. coli* strain BL21-CodonPlus(DE3)RIL competent cells (Stratagene) were transformed by 1 μl of isolated pET-ZZ-TH plasmid as previously described. The cells were then plated on LB-medium with 30 μg/ml kanamycin overnight at 37 °C. One colony from each plate was cultured in 25 ml liquid LB-medium with 30 μg/ml kanamycin until the cell density had reached an optical density at 600 nm of 0.6. The cultures were then split and recombinant protein production was induced in only one of each culture by adding isopropyl thiogalactoside (IPTG) to a final concentration of 1 mM. 1 ml was taken out of each culture after 3.5 hours induction and harvested by centrifugation at 10 000 rpm for 2 min. The bacterial pellet was resuspended in 300 μl of supernatant and the expression of recombinant TH was evaluated by sodium dodecyl sulfate polyacrylamide gel electrophoresis (SDS-PAGE) as described below. A large-scale culture was set up with 600 μl of each uninduced culture in 300 ml autoinduction medium [43] with 100 μg/ml kanamycin and grown at 37 °C an 200 rpm for 2 hours and then at 28 °C and 200 rpm overnight.

4.1.5 Purification of TH

The big cultures were harvested by centrifugation for 15 min at 4°C and 4000 rpm in 1 l tubes, resuspended in a smaller volume and transferred to 50 ml centrifuge tubes. After a second centrifugation, the bacterial pellets were weighted and frozen at -20°C until further use. After thawing, the pellets were resuspended in TALON equilibration/wash buffer (20 mM $Na_2HPO_4 \cdot 2\,H_2O$, 300 mM NaCl, 1 μg/ml pepstatin) using 10 ml/g pellet. Phenylmethanesulfonylfluoride (PMSF), a protease inhibitor, in iso-propanol was added to the dissolved cell pellets to a final concentration of 1 mM before they were sonicated with 9 sec pulses 3 times for 45 sec with 45 sec of pause in between at 20 output Watts while kept on ice. The sonicate was centrifuged 30 min at 4°C and 14 000 rpm to remove cell debris and insoluble material. The fusion protein ZZ-TH was isolated by metal affinity chromatography from the crude extract as following. The crude extract was diluted 1:3 with TALON equilibration/wash buffer and applied to an equilibrated column containing TALON superflow metal affinity resin with a syringe having a filter of 0.45 μm pores.The flow through was allowed to pass through the column twice. The column was then washed with equilibrium/wash buffer until the fusion protein was eluted with 150 mM imidazole. Small samples were taken at each step for evaluation by SDS-PAGE. The buffer was exchanged on a PD-10 column equilibrated with equilibration/wash buffer to remove imidazole. Isolated ZZ-TH was cut with tobacco etch virus (TEV) protease (25-27 kDa) at the optimised conditions of 16 hours at 4°C at a TEV/ZZ-TH (w/w) ratio of 1:50. The cut samples were applied to a second TALON column. The flow through and the first bed volume of the wash were collected, pooled and upconcentrated with amicon filters of 50 kDa cut-off, with FPLC buffer to obtain a sample of purified TH of highest possible concentration. Here again, small samples of each step were collected and evaluated by protein concentration measurements and SDS-PAGE. Pefabloc, a protease inhibitor, was added at a final concentration of 0.5 mM before the sample was stored in liquid nitrogen. The whole purification procedure was carried out in a cooling room at 4°C.

4.2 Gel electrophoresis

4.2.1 Agarose gel electrophoresis

To determine the size of a deoxyribose nucleic acid (DNA) fragment, an electrophoresis was performed on a 10% agarose gel. The 10% (w/v) agarose gel was made by adding 40 ml of TAE buffer to 0.40 g of agarose. The agarose was completely dissolved by heating in the microwave and left to cool down to approximately 50°C before 4 μl of GelRed Nucleic

Acid Stain was added. All was poured into a mold and left to polymerise. 2 μl of 6 x loading dye was added to 10 μl of each PCR product and loaded onto the wells of the gel. The electrophoresis was run in TAE buffer at 100 V for approximately 1 hour. The DNA fragments can be imaged when illuminated by UV light. Pictures were taken of each gel by a ChemiDoc XRS+ (BioRad) using ImageLab 3.0.1 beta 2 software.

4.2.2 Sodium dodecyl sulfate polyacrylamide gel electrophoresis

To determine the presence and the size or the purity and the size of the protein, an SDS-PAGE was performed on a pre-cast 10% (w/v) polyacrylamide gel (BioRad). 15 μl of the samples were denatured by adding 5 μl 4 x loading buffer and incubation of 5 min at 95°C. They were spun down at room temperature and loaded into the wells of the gel next to a low molecular weight standard. The gel was run in a tank buffer at 20 mA for 60 min and afterwards stained with Coomassie Blue. The gel in the staining solution containing Coomassie Blue were heated in the microwave for 30 sec and then left for 10 min on a Belly Dancer (Stoval Life Science). It was then rinsed with destilled water and destained. The gel in the destaining solution was heated in the microwave for 30 sec and then left on a Belly Dancer for 3 hours. Pictures were taken of each gel by a ChemiDoc XRS+ (BioRad) using ImageLab 3.0.1 beta 2 software.

4.3 Size exclusion chromatography

The attachement between the NP^+s and TH was evaluated by size exclussion chromatography (SEC) which is also called gel filtration. At the same time, the NP-TH samples were improved by this procedure non-boun TH which remains in solution is separated from the TH attached to the NPs. A glass econo column (1 cm x 30 cm; Bio-Rad) was packed with ultrogel AcA 34 (Pall Life Sciences) as described by the provider. The separation range of the gel is 20 to 350 kDa into which a TH monomer of 56 kDa falls within. The column was mounted in a Bio-Logic Duoflow system and calibrated with standards to identify the elution volume of front and the end of the column.

Prior to all SEC experiments, the column was equilibrated with fast protein liquid chromatography (FPLC) buffer (20 mM HEPES, 200 mM NaCl, pH 7.0), the UV lamp is switched on 30 min in advance for equilibration, and the sample loop is flushed with three times its volume, using FPLC buffer as the running buffer. The parameters used here are a maximum pressure, limited by the ultrogel, of 7 psi and a flow rate of either 0.25 ml/min or 0.5 ml/min, depending on the sample. Fractions were collected with a

Bio-Logic Bio-Frac Fraction Collector (Bio-Rad). This SEC procedure was only done for NP^+s, since $DPPGNP^+$s were suspected to contaminate the column or the tubings, and with many users of the Bio-Logic system this could not be risked.

4.4 Dynamic light scattering

To determine any change in the size of the NPs upon the presence of TH, titrations were performed by adding increasing amounts of diluted TH to a solution of NPs. At first, the stock TH was diluted in FPLC buffer to a concentration of 1 mg/ml. NP^+ and $DPPGNP^+$ were diluted to 0.5 mg/ml in FPLC buffer. The diluted TH stock was gradually added to the NPs in solution and the titration samples were each time scanned in a low volume quartz cuvette 12 μl (Hellma Analytics) in a Nanosizer S (Malvern Instruments) at 25°C using 173° backscatter angle, a refractive index of 1.330. To estimate the effect of dilution on the DLS measurements, control samples were prepared by adding only water to the nanoparticles.

4.5 Atomic force microscopy

The surface of the NPs was studied with AFM to observe if a structural change occured on the surface of the NPs when TH was attached. A mica sheet (Agar scientific) surface was cleaned by ripping off a complete layer with some Scotch Magic tape and fastened to a microscope slide. 10 μl containing 0.05 mg/ml NP and 0.02 mg/ml TH was dripped on the mica surface while keeping the microscope slide tilted so that the droplet spreads over the mica surface. The sample was dried for 60-90 min under an upside down glass beaker to prevent it from dust. The fresh sample was scanned with an ACT cantilever (AppNano) having a tip radius of < 10 nm, a resonant frequency between 200 - 400 kHz and a spring constant between 25 and 75 N/m. The scanning was done in an MFP-3D AFM (Asylum research) which is mounted on an anti-vibration table (Halcyonics), using a tapping mode, a -5% target frequency, a scan rate of 1 Hz, a set point of around 200 mV, an integral gain of 7 and a drive amplitude of 120 mV. The images were acquired with Igor Pro software (Wavemetrics, Inc.) and the height image was flattened while excluding a mask covering the NPs in the modify panel. A line was drawn across the image to plot the height profile in a 2-D graph by using the draw function in the analyse panel.

4.6 TH activity assay

The specific activity of TH (nmol L-DOPA/min/mg) was measured by the use of 3',5'-^{3}H-tyrosine according to the protocol previously described by Reinhard [44]. In this assay, the number of radioactive water molecules produced in the catalysis equals the number of L-DOPA molecules (Figure 4.2), which are filtered away together with unused radioactive L-tyrosine through activated charcoal and posterior precipitation by centrifugation. The more active TH present, the more radioactive water there will be in the sample.

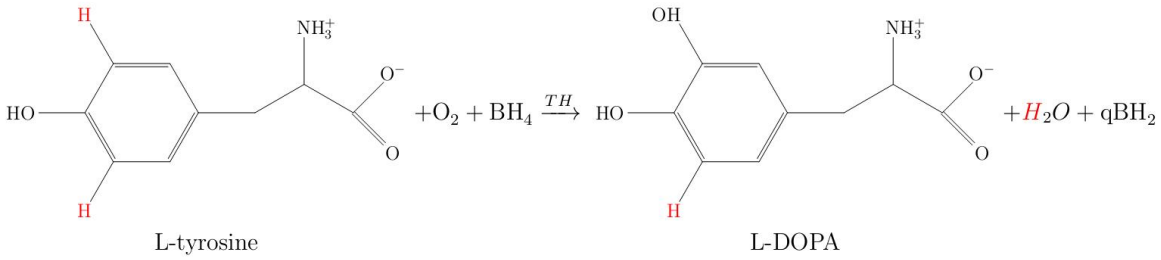

Figure 4.2: Reaction in the tyrosine hydroxylase (TH) activity assay. L-tyrosine is labelled with radioactive tritium at two positions. One of these tritiums is substituted by an hydroxyl group to give L-3,4-dihydroxyphenylalanine (L-DOPA) and the other tritium atom ends up in a water molecule. Tritium is displayed as a red hydrogen atom since it is an isotope of hydrogen.

The conditions in the assay were 0.1% (w/v) BSA, 100 mM HEPES buffer pH 7.0, 50 μM L-tyrosine, 20 μM Fe^{2+} and 0.05 mg/ml catalase. First 2 ng/μl TH was pre-incubated in this mixture for 1 min at 37°C, then 500 μM BH_4 in 5 mM DTT was added to initiate the reaction and incubated for 4 additional min at 37°C. The reaction was stopped with an excess of charcoal (7.5% (w/v) in 1N HCl).

Prior to each activity assay, TH was thawn in the cryotube, centrifuged 10 min at 4°C and 10000 rpm and the supernatant tranferred to a new tube. The protein concentration of the supernatant was determined by measuring the absorbance at 280 nm measured in the nanodrop (Saveen Werner) , based on the extinction coefficient for 1% TH = 8.14, and using FPLC buffer as blank measurement.

The specific activity was always measured as a time scan. Each sample was incubated at 37°C and a small volume was taken out at 2 min, 1 h and 24 h for the assay to determine the activity at that specific time. The assay itself takes only 5 min per sample (Figure 4.3) and each condition was tested twice, with the second parallel having a 30 sec delay in comparison to the first parallel. The results are presented as a means of the two parallels ± standard deviation.

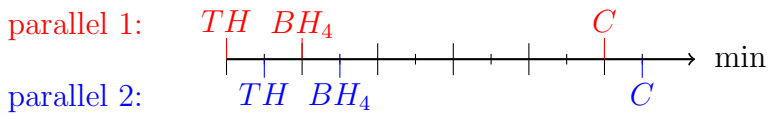

Figure 4.3: Time line of the tyrosine hydroxylase assay with two parallels simultaneously

4.7 Protein labelling with fluorescent dye

3 mg TH at a concentration of 2 mg/ml was labelled at a 10% (w/w) with fluorescein isothiocyanate (FITC). The labelling was done in a carbonate buffer of pH 9 by combining sodium bicarbonate ($NaHCO_3$) and sodium carbonate (Na_2CO_3). The basic environment was neutralised after 4 hours by the addition of PBS. Free FITC was separated from labelled TH by size exclusion chromatography using a Amersham Biosciences PD-10 desalting column. This labelling procedure was carried out in the lab of Didier Betbeder, Univerversite de Lille 2, France. Alternatively, as done in Bergen, TH was labelled by covalent attachment of Alexa Fluor 568 (Alexa) according to manufacturer's instructions. Basically, TH was labelled in a FPLC buffer supplemented with sodium bicarbonate to a basic solution of pH 7.5 –8.5 and at a concentration of 2 mg/ml. 1 mg TH was incubated with Alexa for 1 h at room temperature and then purified through a column containing Bio-Rea BioGel P-30 Fine size exclusion purification resin to separate labelled protein from free dye. The absorbance of Alexa-TH at 230 and 280 nm was measured, allowing the calculation of the concentration (equation 4.1), where c is the concentration of the labelled protein sample, M_W the molecular weight of the protein, A the absorbance and ϵ_{280} the extinction coefficient at 280 nm.

$$c(mg/ml) = c(M) * M_W(g/mol) = \frac{[A_{280} - A_{230} * 0.46](A.U./cm) * M_W(g/mol)}{\epsilon_{280}(cm^{-1} * M^{-1})} \quad (4.1)$$

4.8 Cell cultures

Human bronchial epithelial 16HBE14o- (HBE) and human epithelial NCI-H292 (H292) cell lines were grown in Dulbecco's Modified Eagle Medium supplemented with 10% (v/v) fetal bovine serum (FBS), 1% (w/v) glutamine (Gln), 100 U/ml penicillin and 100 μg/ml streptomycin. Rat adrenal pheochromocytoma PC12 cell line was grown in Roswell Park Memorial Institue medium (RPMI) supplemented with 10% (v/v) horse serum, 10% (v/v) bovine serum, 2 mM Gln and 1 x penicilin and streptomycin mix. Human embryonic kidney HEK293 cell line was grown in DMEM supplemented with 10% (v/v) FBS, 2 mM

Gln and 10 U/ml antibiotic mix. Cells were grown as monolayer in T_{75} flasks or P_{100} plates (Sarstedt) with 10 ml medium at 37°C in 5% CO_2 and a humidified atmosphere. Cell culture work with the two types of epithelial cells was performed during a two weeks stay in the lab of Didier Betbeder, Université de Lille 2 in France, whereas the work with PC12 and HEK293 was performed in Bergen.

At confluence, the cells were splitted: The HBE and H292 cells were washed with PBS and detached with 0.02% (w/v) trypsin for 5 min. Cells were collected by centrifugation (5 min at 22°C and 1500 rpm), resuspended in complete DMEM and seeded in a dilution of 1:3. PC12 cells were mechanically detached by light tapping of the surface and subsequently disaggregated by repeated pipetting and forcing cells through a BD microlance 3 21G needle (0.8 x 40 mm) coupled to a 1 ml syringe. PC12 were seeded in a dilution between 1:12 to 1:2. HEK293 cells were washed with PBS, detached by treatment of a solution containing 0.25% (w/v) trypsin and 1 mM ethylenediaminetetraacetic acid (EDTA) (max 5 min) and seeded in a dilution between 1:12 to 1:2 in complete DMEM.

At 60–70% confluence, the cells were detached and centrifuged 5 min at 4°C and 1250 rpm in 6 ml complete medium. The pellet was resuspended in complete medium supplemented with 10% (v/v) dimethyl sulfoxide (DMSO) and frozen to −80°C at a rate of 1°C/min. After 48 to 72 h at −80°C, and posteriorly stored in liquid nitrogen.

4.8.1 Cellular model of protein delivery

A cell model for delivery studies was created by using cells in suspension during a splitting. HBE and the H292 cells were seeded in 8-well Lab-Tek chamber slides in a 1:3 dilution and the cells in the wells were grown for 24 h to develop a monolayer. PC12 and HEK293 cells were seeded at 100000 cells per well in 4-well plates (Nunc) that contained glass coverslips previously coated with 0.01% (w/v) poly-lysine in PBS for 45 min at 37°C. These cells were also grown 24 h before starting experiments.

4.8.2 Sample preparation for confocal microscopy

The nuclei of the HBE cells were labelled with 0.1% (w/v) 4',6-diamidino-2-phenylindole (DAPI) for 5 min at room temperature (RT) and then 400 μl PBS containing 10 μg NPs and approximately 3.5 μg TH was added and live imaging was performed immediately.

TH was incubated 10 min at room RT with each type of NPs in an approximate 1:3 (w/w) ratio before the solution was diluted in PBS. All cells except HBE, were washed with PBS and incubated 1 h, or longer with 400 μl PBS containing approximately 3.5 μg fluorescent TH and 10 μg NP at 37°C in 5% CO_2 and a humidified atmosphere.

The NP-treated H292 cells were washed with 4°C PBS and therafter fixed to the bottom of the wells by 4% (w/v) para-formaldehyde (PFA) for 10 min at RT. Cell nuclei were stained with DAPI for 5 min at RT and cells were washed twice with 400 μl PBS and once with distilled water. The cells were left in water for imaging.

The NP-treated PC12 and HEK cells were washed with 400 μl 4°C PBS and the cells fixed to the glass coverslip by 10 min incubation with 4% (w/v) PFA at RT. The cells were again washed twice with PBS and then once with distilled water. After removing the water, the coverslips were mounted facedown on microscope slides using Prolong Gold with DAPI antifade reagent (Life technologies) and left to harden overnight at RT. Confocal imaging was subsequently performed.

4.9 Confocal microscopy

All samples were imaged with a Zeiss LSM 710 or Leica TCS SP5 laser scanning confocal microscope using a HCX PL Apo lamda blue objective with magnification of 63x, numerical aperture 1.40, oil immersion and a working distance of 0.1 mm. Fluorescent FITC-TH was excited with the 488 nm laser line from an Argon laser, whereas fluorescent Alexa-TH was excited by a 561 nm laser line from a DPSS laser. DAPI stain was excited using a 405 nm laser line from a laser diode. In all cases, the laser power was adjusted to minimise photobleaching.

Zoom and field dimensions were adjusted to give a pixel size of approximately 100 nm. Single plane images were taken when most of the cell nuclei were in focus. Z-stacks were acquired every 0.34 μm starting at the coverslip surface and ending when the cell monolayer was out of focus. Images were processed using Fiji (freeware).

5 Results

5.1 Recombinant tyrosine hydroxylase (TH)

5.1.1 TH from MBP-TH fusion protein

TH was usually expressed as an MBP-TH fusion protein and the typical yield was 5 - 10 mg from 6 l bacteria cultures. TH-MBP was then cleaved by restriction protease factor Xa at a 1:200 (w/w) ratio between factor Xa and TH-MBP. Cleaved, soluble TH was separated from aggregates and the fusion partner MBP by size exclusion chromatography on a HiLoad Superdex column (1.6 cm x 60 cm) as seen in figure 5.1. The fractions 9 to 15 containing the second peak were pooled as they were known to contain tetrameric TH. The pooled fractions were upconcentrated by ultrafiltration with filters with a cut-off of 30 kDa and stored in liquid nitrogen until use.

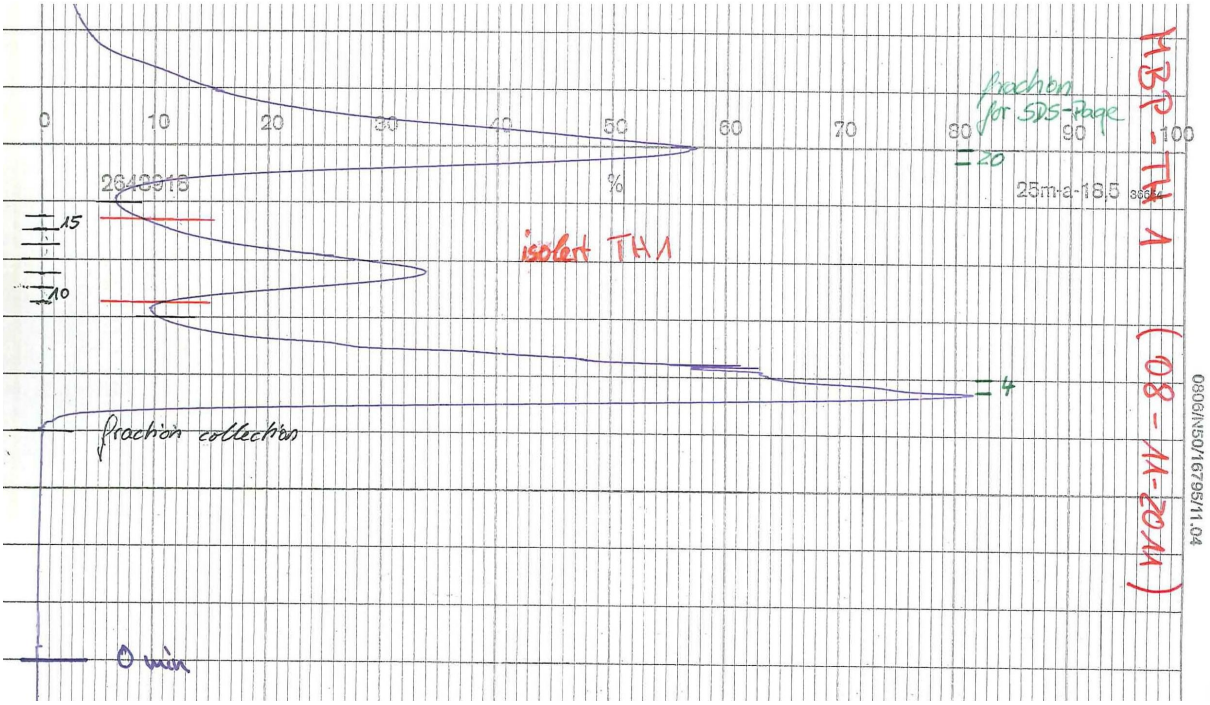

Figure 5.1: Size exclusion chromatography as the last step in the purification of TH from MBP-TH. The first major peak contains aggregates and the third MBP, while pure TH is in fractions 9 to 15, which contain the second peak. These fractions were pooled and up-concentrated.

The size of both the MBP-TH fusion protein and the purified TH has been corrobo-

rated by SDS-PAGE (Figure 5.2a). Results from size exclusion chromatography were also analysed by SDS-PAGE (Figure 5.2b). MBP-TH cleaved by factor Xa before SEC is a sample that consists mainly of two proteins: TH and MBP as two bands can be seen in lane 3 of figure 5.2b.

The first peak from the bottom is the void volume of the column in which particles too big to enter the pores of the column medium are eluted. It was represented by fraction 4 (Figure 5.1) and shows to be mainly TH (lane 4 figure 5.2b) although it is expected that this TH is aggregated. The second peak was a pool of fractions 9 to 15 (Figure 5.1) and corresponded to purified TH with some low molecular weight contaminants (lane 2 figure 5.2b). MBP is eluted at last and is represented by fraction 20 (Figure 5.2b lane 5) that represents the third peak from the bottom in SEC (Figure 5.1).

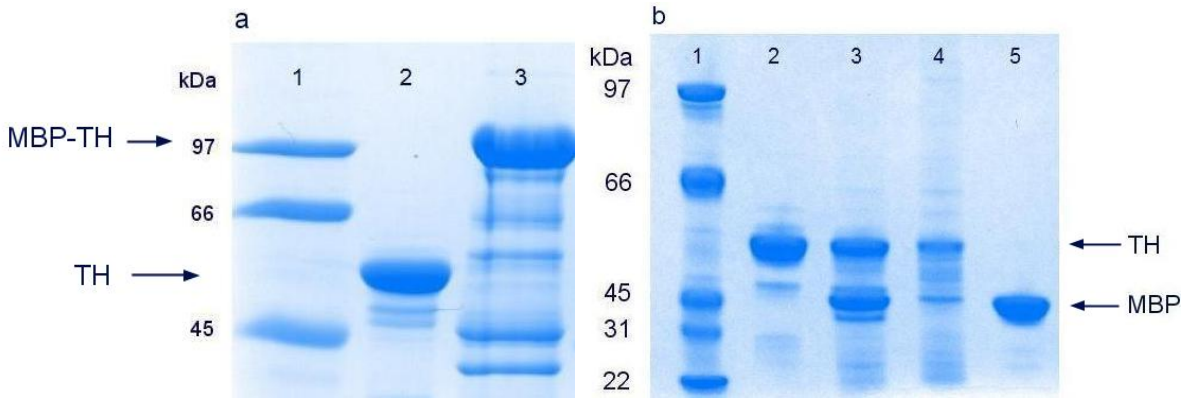

Figure 5.2: SDS-PAGE analysis of the purification of TH from MBP-TH. (a) Evaluation of purification. Lane 1: BioRad Low molecular weight standard. Lane 2: MBP-TH fusion protein. Lane 3: Purified TH by size exclusion chromatography. (b) Effect of size exclusion chromatography. Lane 1: BioRad Low molecular weight standard. Lane 2: TH (56 kDa) purified by SEC from fraction 9 to 15. Lane 3: Cut TH-MBP with restriction protease factor Xa at a 1:200 ratio. Lane 4: Fraction 4 of purification after cutting with factor Xa. Lane 5: Fraction 20 of same purification containing the MBP fusion partner (42.5 kDa).

5.1.2 TH from ZZ-TH fusion protein

Despite the high yield obtained by the procedure using MBP-TH, we appreciated certain heterogeneity in the final TH preparation and increased tendency to aggregate. We hypothesised that this might be caused by unspecific cleavage of the fusion protein. Moreover, the yield of the expression and purification could not be increased further and restriction protease factor Xa is very expensive. For these reasons, a new expression strategy was developed. TH was to be expressed in a fusion protein with a ZZ-carrier and six histidines at its amino terminal (a his-tag). The ZZ-carrier domain increases solubility

and the polyhistidine-tags have an affinity for the metals nickel and cobalt, which can be used for selection during purification by affinity chromatography.

Cloning

First, the *TH* gene was sucessfully amplified by PCR and inserted into the pET-ZZ-1a vector. *E. coli* XL10-Gold ultracompetent cells (Statagene) were transformed with the plasmid containing the gene for TH and colonies were screened for the presence of the *TH* gene. Many colonies had sucessfully been transformed as was confirmed by electrophoresis on a 10% agarose gel after a colony PCR as shown in figure 5.3a.

Two colonies (1A and 1B) were selected for plasmid isolation. The two plasmids were doublechecked after isolation by electrophoresis on a 10% agarose gel as seen in figure 5.3b. It confirms the sucessful insertion as two bands appear with the first band being the plasmid o 5724 basepairs (bp) without the gene and the second (1549 basepairs) TH that was cut out as a test by Acc651 and Nco1. This was predictable as the *TH* gene is 1549 basepairs when it contains the extra ends with the restriction sites for Acc651 and Nco1, as designed by the primers.

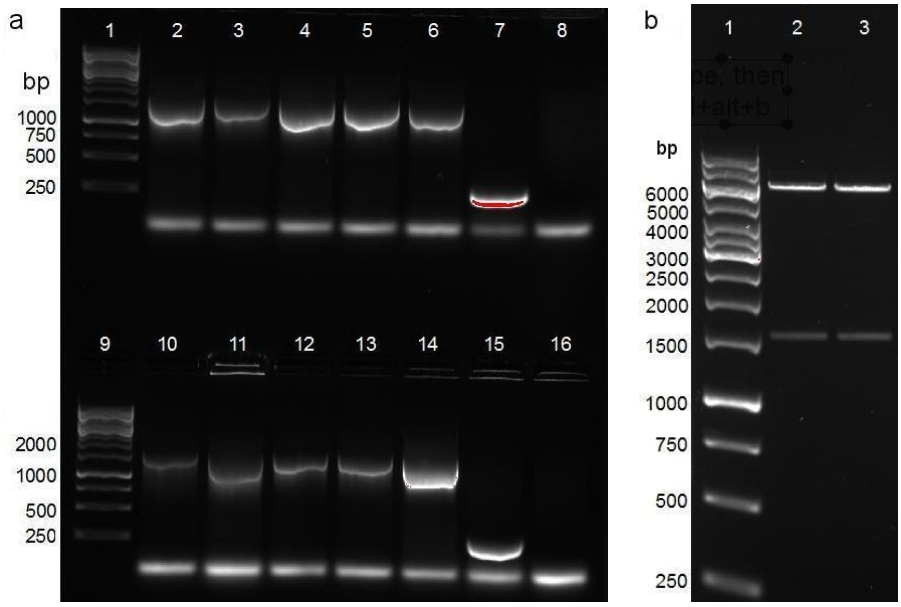

Figure 5.3: Agarose gel electrophoresis. (a) Initial screening for the presence of the of *TH* gene in the transformed colonies. Lanes 1 and 9: 1 kb DNA ladder, lanes 2-7: colonies 1A-6A, lanes 10-15: colonies 1B-6B, lanes 8 and 16: negative controls (from transformations with water instead of ligations). (b) Newly synthesised and isolated plasmids. Lane 1: 1kb DNA ladder. Lane 2: pET-ZZ-1a/hTH1 plasmid isolated from colony 1A and cut with Acc561 and Nco1. Lane 3: pET-ZZ-1a/hTH1 vector plasmid isolated from colony 1B and cut with Acc561 and Nco1.

Expression and purification

Expression of the ZZ-TH (72.5 kDa) fusion protein was observed in the two test cultures that were induced by IPTG (data not shown). The fusion protein was overexpressed in *E. coli* strain BL21-Codon Plus(DE3)RIL (Figure 5.4a lane 2) that were grown in autoinduction medium [43]. Soluble fusion protein was found in the crude extract after sonication and centrifugation to remove cellular debris and insoluble proteins (Figure 5.4a, lane 3). This initial purification showed that, after metal affinity chromatography according to manufacturer's instructions with elution by imidazole, the fusion protein fraction was enriched with low molecular weight contaminants (Figure 5.4a, lane 6). Also, a lot of the fusion protein was lost in the flow-through due to saturation of the column (Figure 5.4a, lane 5). A cutting test could however be performed on the eluated ZZ-TH. After buffer exchange, the ZZ-TH fusion protein was cleaved at different (w/w) ratios by Tobacco etch virus (TEV) protease. At a 1:10 (w/w) ratio between TEV and ZZ-TH, complete cleavage was obtained at all incubation times (Figure 5.4b lane 2, 3 and 4).

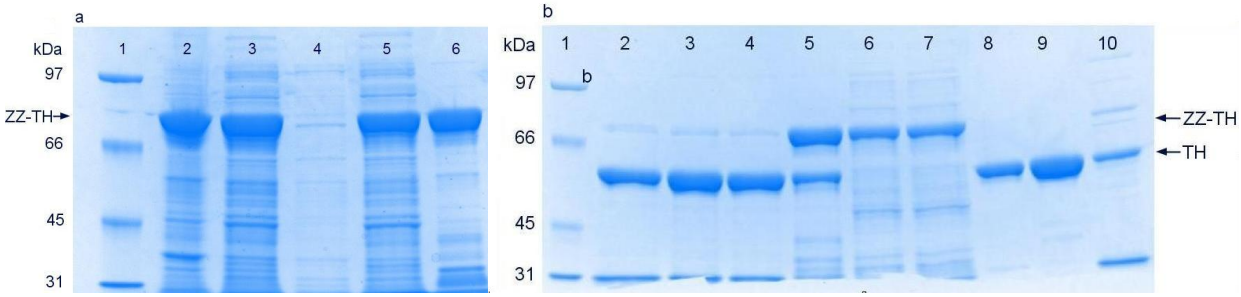

Figure 5.4: SDS-PAGE of the expression and purification of TH from ZZ-TH. (a) SDS-PAGE analysis of the presence of ZZ-TH (72.5 kDa). Lane 1: BioRad Low molecular weight standard. Lane 2: *E. Coli* cell pellet. Lane 3: Crude extract of transfected *E. Coli*, after sonication and centrifugation. Lane 4: Early flow through of first TALON column. Lane 5: Late flow through of first TALON column. Lane 6: Eluate of first TALON column. (b) An SDS-PAGE analysis of the cutting test and the purification. Lane 1: BioRad Low molecular weight standard. Lane 2: TEV cleavage of ZZ-TH at 1:10 (w/w) ratio an 3.5 h incubation. Lane 3: TEV cleavage of ZZ-TH at 1:10 (w/w) ratio and 6 h incubation. Lane 4: TEV cleavage of ZZ-TH at 1:10 (w/w) ratio and 17.5 h incubation. Lane 5: TEV cleavage of ZZ-TH at 1:100 (w/w) ratio and 17.5 h incubation. Lane 6: Early flow through of first TALON column. Lane 7: Late flow through of first TALON column. Lane 8: TH that has been cleaved by TEV at a 1:50 TEV/ZZ-TH ratio for 16 h. Lane 9: FLow through of second TALON column, corresponding to purified TH. Lane 10: Eluate of second TALON column.

The bed volume of the TALON resin was then increased until 20 ml so that much less was lost, although some loss of ZZ-TH could not be completely avoided (Figure 5.4b lanes 6 and 7). After buffer exchange to remove the imidazole, the ZZ-TH fusion protein was completely cleaved by Tobacco etch virus (TEV) protease at an optimised ratio of 1:50 (w/w) between TEV and ZZ-TH (Figure 5.4b lane 8) and TH was purified by a second

round on the TALON column where TH is found in the flow through (Figure 5.4b lane 9). His-tagged ZZ fusion partner is retained in the column and eluted with imidazole before regeneration of the resin (Figure 5.4b lane 10). The homogeneity of this preparation of purified TH was found to be satisfactory.

5.1.3 TH labelling

To visualise the localisation of TH in cells, TH needed to be labelled with a fluorescent dye. First, FITC was covalently attached to TH by an incubation at high pH. Successfully labelled TH was separated from non-bound FITC by SEC using a PD-10 column (GE Healthcare), during the purification a clear area could be observed between an orange band containing TH and the yellow band of FITC. Fluorescence of small fractions from the purification confirmed these results (data not shown). Later, TH was also labelled successfully with Alexa as the purple band of labelled TH and the pink band of Alexa were clearly separated from each other during the purification SEC. The absorbance of Alexa-TH was measured at 230 and 280 nm and the concentration of the labeled protein was then calculated according to equation 4.1 to be 1.73 mg/ml.

5.1.4 Enzymatic activity of recombinant TH

The enzymatic activity of TH was measured after cleavage from TH-MBP or from ZZ-TH or after labelling giving Alexa-TH (Figure 5.5). This was to compare the two expression methods and to see if labelling reduced the activity.

The initial activity of TH seems similar for both TH from MBP-TH, from ZZ-TH and for Alexa-TH as the differences were found not to be significant, as seen roughly, the variations fall within eachother's standard deviation (SD). Typically, the activity decreases over time. TH from MBP-TH has only half of the activity left after 1 h. TH from ZZ-TH however seems to loose its activity much slower as very little (only around 10%) is lost after the first hour of incubation. After 24 h, the activity has decreased to below 50 nmol L-DOPA/min/mg TH for all samples.

5.2 Binding of TH to nanoparticles (NPs)

5.2.1 Separation of free and bound TH

NP^+ was incubated with TH for at least 10 min on ice and then bound and unbound TH were separated by SEC (Figure 5.6b) using a Glass Econo-Column (diameter: 1

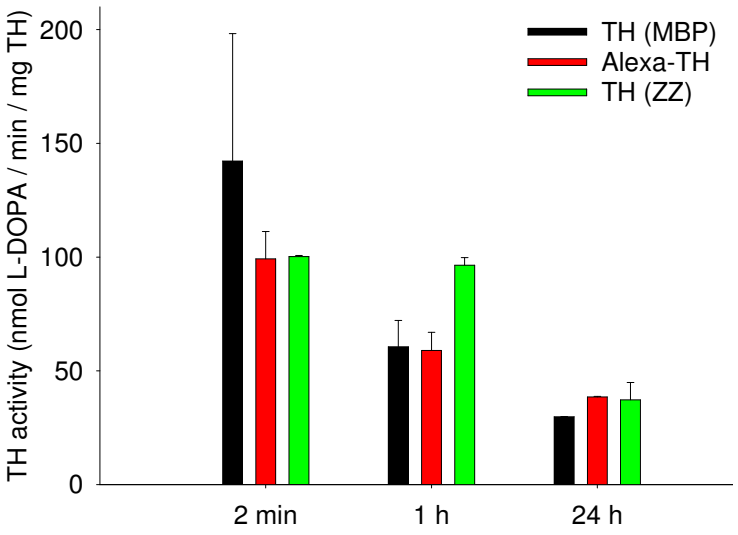

Figure 5.5: Comparison of TH activity for TH expressed and purified by different methods, over time at 37°C.

cm; length: 20 cm) packed with Ultrogel AcA 34 media. To calibrate and to check the homogeneity of the column, a mixture of blue dextran (2000 kDa), thyroglobulin (500 kDa) and adenosine monophosphate (AMP; 0.347 kDa) was added. Blue dextran is know to elute in the void volume [45], which is also the front of the chromatogram (9.5 ml) and AMP elutes in the total column volume (24 ml) (Figure 5.6a). Cytochrome c eluted between the front and end peaks as its size (49 kDa) lies within the separation range, while thyroglobulin is not properly separated from blue dextran.

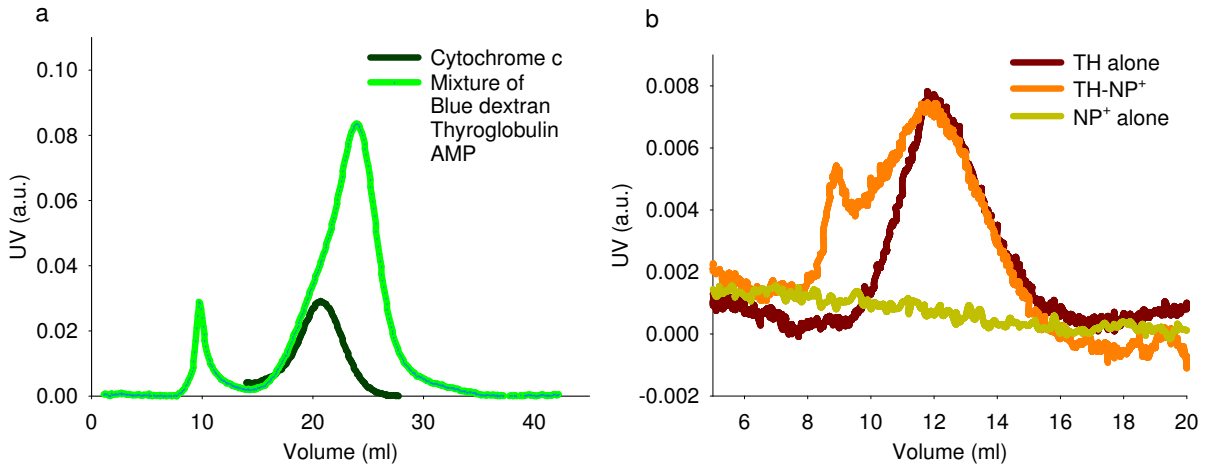

Figure 5.6: Size exclusion chromatography with AcaGel 34. (a) Calibration. (b) Separation.

TH gives a clear peak in the separation range, which can be seen in figure **??**. The sample with NPs and TH gives two peaks, one for the NPs loaded with TH, which are

so big that they come in the void volume and one for the unbound TH in solution. The second peak overlaps almost completely with the peak when TH is run alone.

The enzymatic activity was tested, to see if SEC changed TH's activity (Figure 5.7). When TH was run alone through the Ultrogel AcA 34 packed column as a controll, its initial activity was at an average of 308 nmol L-DOPA/min/mg which does seem only slightly lower than usual and could be included in the variation from day to day of initial TH activity. The TH that is bound to NP^+ seems much less active. A possible reason is that TH is contained in the pores of NP^+ so that its active site is not available for conversion of L-tyrosine to L-DOPA. However, this activity seems to be maintained over time.

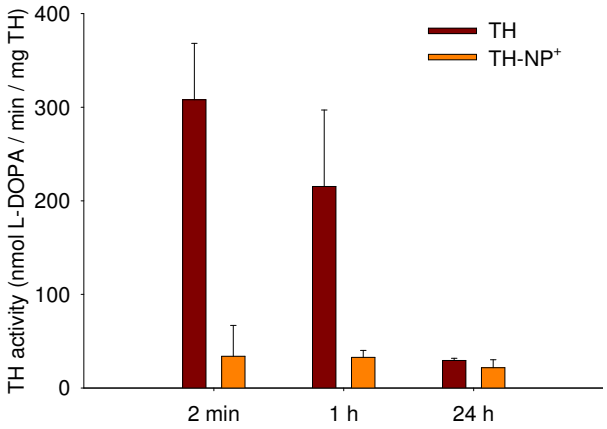

Figure 5.7: TH activity of TH alone (dark blue) and TH when bound to NP^+ (light blue) after size exclusion chromatography through an Ultrogel AcA 34 packed column. Incubations were performed at 37 °C.

5.2.2 Evaluation of NP-bound TH

To evaluate the NP-bound TH, a small sample of the fraction containing the first peak appearing in the separation spectrum was loaded on a 10% polyacrylamide gel next to a control of TH from SEC of the same concentration (Figure 5.8). To ensure correct concentration measurements, the NP^+s were also measured alone, but gave no signal (data not shown) as expected, since the absorbance at 280 nm is typical for proteins. Almost none of the NP-bound TH was denatured by SDS as can be seen by the weakness of the band in the left lane, even though the protein amount loaded on the gel was the same as free TH (right lane). NP^+ seems to have protected TH from denaturation and solubilisation and prevented the entering into the gel. NP^+ loaded with TH seemed to have been left in the well. This indicates that the binding was successful. The weak band

suggests that there is an equilibrium between the bound TH and free TH and that some can therefore be released.

Figure 5.8: Comparison of TH bound to NP^+ (left lane) and free TH (right lane).

5.2.3 Size determination

To evaluate the binding between TH and the two types of NPs, a titration with increasing amounts of TH was done and followed by DLS. The temperature during all measurements was kept at 25°C. To ensure that the size increase was not due to a side effect of the inevitable dilution during the titration, a dilution control (c) was performed. All measurements were done in triplicates. The results show that the average diameter of both types of NPs increases steadily with increasing TH concentration, whereas the dilution controls remain approximately constant (Table 5.1, figure 5.9).

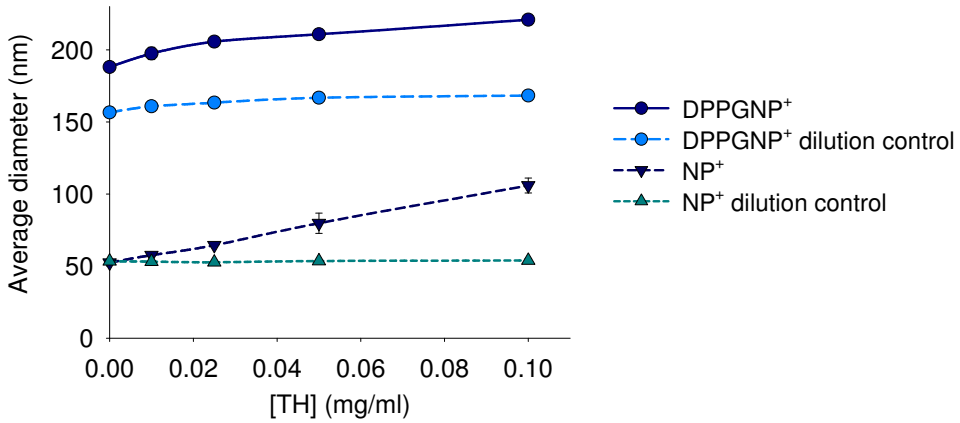

Figure 5.9: The average nanoparticle diameter versus TH concentration.

The first size increase which happens at a TH concentration of 0.01 mg/ml seems quite small, only 5.21 nm (Table 5.1) compared to the size of TH in solution which is approximately 12 nm (data not shown). The NPs are proposed to be porous [29] so the enzyme could be partly included in the pores. The dilution control deviates by only 1.02 nm from the average diameter (Tables 5.1) for NP^+. There can also be observed a gap between the initial size measurements of DPPGNPs depending on if it is part of the titration or of the dilution control. The sizes for DPPGNP and its dilution control do

Table 5.1: Titration of NP-samples with increasing amounts of TH, followed by DLS

Sample	[TH] (mg/ml)	Z-ave (nm)	± (nm)	PdI
NP-1	0.00	52.33	0.2970	0.167
NP-2	0.01	57.54	0.4405	0.25
NP-3	0.025	64.42	0.4518	0.268
NP-4	0.05	79.73	7.031	0.403
NP-5	0.10	105.9	5.173	0.525
NP-1 c	-	53.35	0.4172	0.186
NP-2 c	-	53.05	0.5405	0.180
NP-3 c	-	52.65	0.2139	0.182
NP-4 c	-	53.50	0.8884	0.185
NP-5 c	-	53.86	1.496	0.206
DPPGNP-1	0.00	188.1	2.836	0.282
DPPGNP-2	0.01	197.5	4.289	0.268
DPPGNP-3	0.025	205.7	3.528	0.274
DPPGNP-4	0.05	210.8	0.9504	0.284
DPPGNP-5	0.10	220.9	1.762	0.266
DPPGNP-1 c	-	156.6	3.190	0.260
DPPGNP-2 c	-	160.9	2.955	0.284
DPPGNP-3 c	-	163.4	3.424	0.276
DPPGNP-4 c	-	166.8	2.281	0.272
DPPGNP-5 c	-	168.3	1.308	0.263

not correspond at the beginning of the measurement. One plausible reason could be the effect of the ions in the buffer solution which affect the ordering of the lipids.

5.2.4 Visualisation of the nanoparticles containing TH

To observe any structural change to the surface of the NPs upon TH attachement, the NPs were scanned by AFM. 10 μl droplets of NP samples were spread on mica which was fastened to a microscope slide. The NP concentration was optimised to 0.05 mg/ml as that gave a monolayer of particles with such spacing between them that was suitable for imaging. When TH was present in the sample, its final concentration was 0.02 mg/ml. Dilutions were done i water as buffer and salt increased crystal formation and high background in the AFM images. Crystals could still be observed in many samples and the areas that were scanned were selected such that they did not contain crystals, but rather have a suitable spacing between NPs.

The imaging was done after drying the sample drop on the mica for 60-90 min. All samples were imaged three times at three different spots on the slide to ensure that the

pictures are representative. An overview image of either 20 μm $\times$ 20 μm or 5 μm $\times$ 5 μm was always scanned first before a 1 μm $\times$ 1 μm zoom was made. The best images were selected and their height profiles analysed.

NP^+ is seen as a red spot in the height image with a yellow background (Figure 5.10a) meaning that it is higher than the rest of the sample surface. And when its dimensions are analysed from height profiles like the one in figure 5.11, the diameter is 190 nm and the height is 5 nm. NP^+ can also be seen in both the amplitude (Figure 5.10b) and the phase (Figure 5.10c) images. The background seems to have a pattern reminding of a knitted jumper. This is the structure of the mica surface because it is exactly what is seen when only the mica surface is imaged (data not shown).

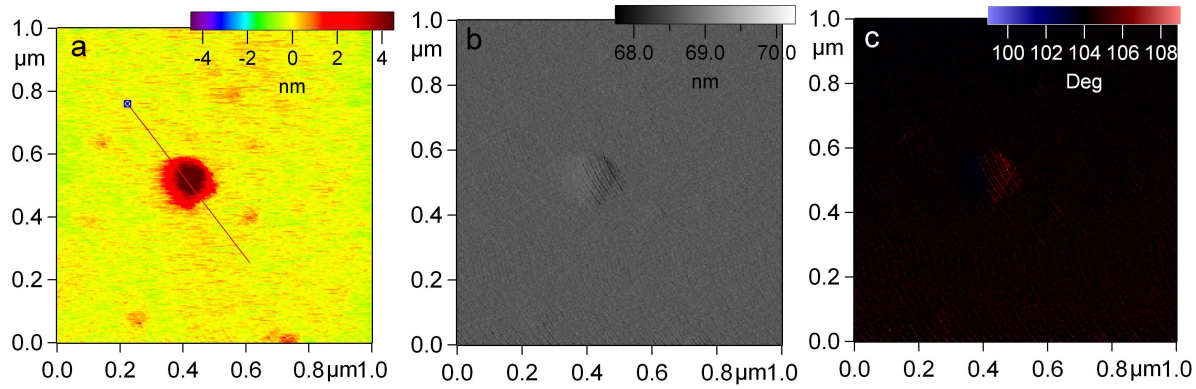

Figure 5.10: NP+ imaged by AFM in (a) height, (b) amplitude and (c) phase mode.

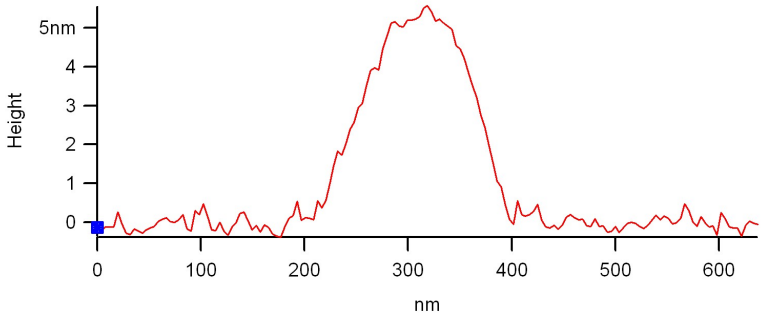

Figure 5.11: Height profile of NP^+

$DPPGNP^+$ gave similar results to NP^+ (Figure 5.12) although these lipid containing NPs look a bit like fried eggs with a thin bottom level and a thicker core. This is especially visible in the amplitude mode (Figure 5.12b) The height profiles (like figure 5.13) give larger dimensions than for NP^+ which is as expected. The bottow level has a diameter of almost 400 nm and a height of 4 nm and a top level of 200 nm in diameter and 6 nm high.

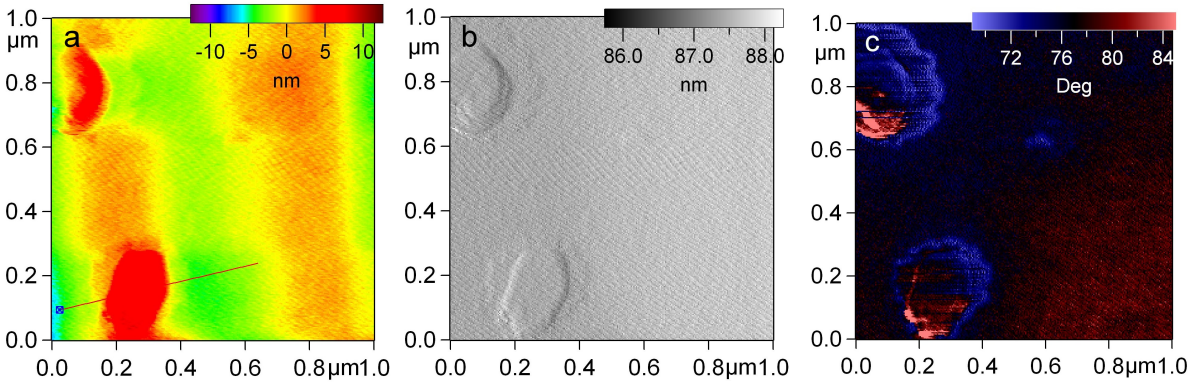

Figure 5.12: DPPGNP+ imaged by AFM in (a) height, (b) amplitude and (c) phase mode.

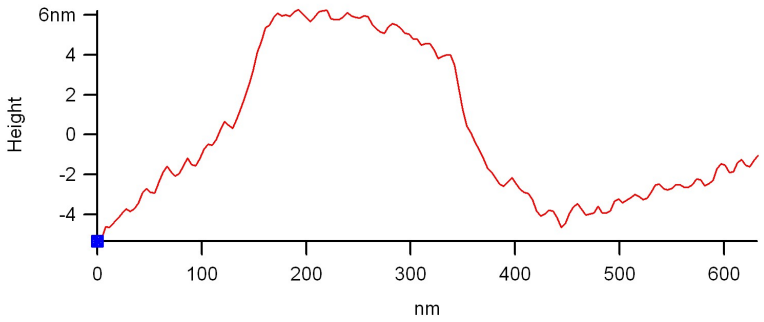

Figure 5.13: Height profile of DPPGNP$^+$

When NP$^+$ are loaded with TH, the background in the images appeared to have changed independent of the visualisation mode (Figure 5.14). The NP$^+$ are still comparable in size although the height is now 8 nm (Figure 5.15) instead of 5 nm. It is difficult to say if this change is due to the presence of TH or not. The diameter even seems a little smaller: 170 nm instead of 190 nm. TH could give the porous NP$^+$ more rigidity so that the AFM scan comes closer to the real dimensions. The phase image (Figure 5.14c) shows a dark area where the NP$^+$ loaded with TH is located. TH seems therefore to change the phase in the opposite direction than what NP$^+$ itself does.

The background is crowded when DPPGNP$^+$s loaded with TH are imaged (Figure 5.16). It is difficult to know if this represents aggregated NPs or only TH which also might be aggregated to give larger structures than its own size. Some blue spots can be observed in the phase image. The DPPGNP$^+$ loaded with TH seems 12 nm in height and 350 nm in diameter according to one of the height profiles (Figure 5.17).

NP$^+$s loaded with TH after separation from unbound TH by SEC provide a much flatter background (Figure 5.18) than when the sample of TH bound to NP$^+$ was not gel filtrated to take away unbound TH (Figure 5.14). This is better appreciated in the heigth profile (Figure fig:NP+THSECS). However gel filtration also seems to have taken away

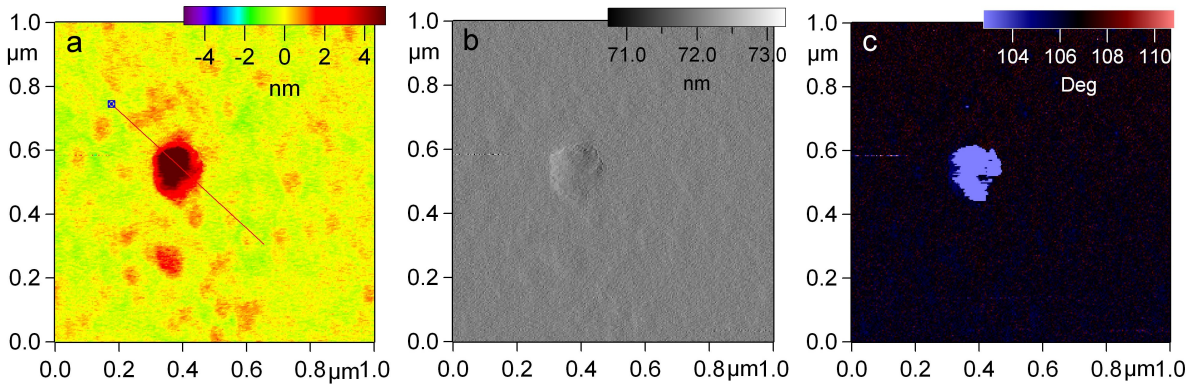

Figure 5.14: NP^+ with TH imaged by AFM in (a) height, (b) amplitude and (c) phase mode.

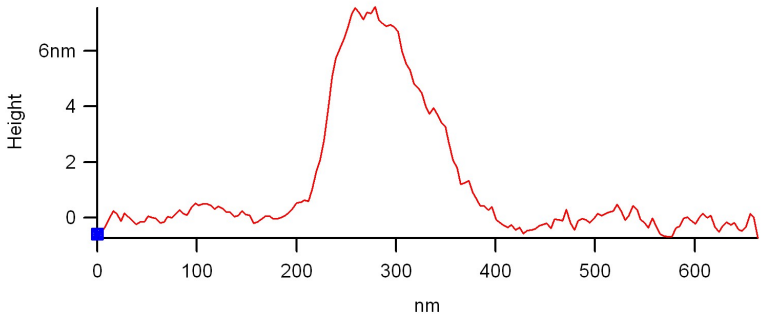

Figure 5.15: Height profile of NP^+ with TH.

some of the loaded TH as the phase image (Figure 5.18c) shows less dark areas on the particle itself. This can explain the huge decrease in activity when TH is bound to NP^+ and all unbound TH is removed by SEC.

The maximum height that can be read from the profile is 30 nm for this sample and this seems more reasonable than the value obtained previous to filtration, which was 12

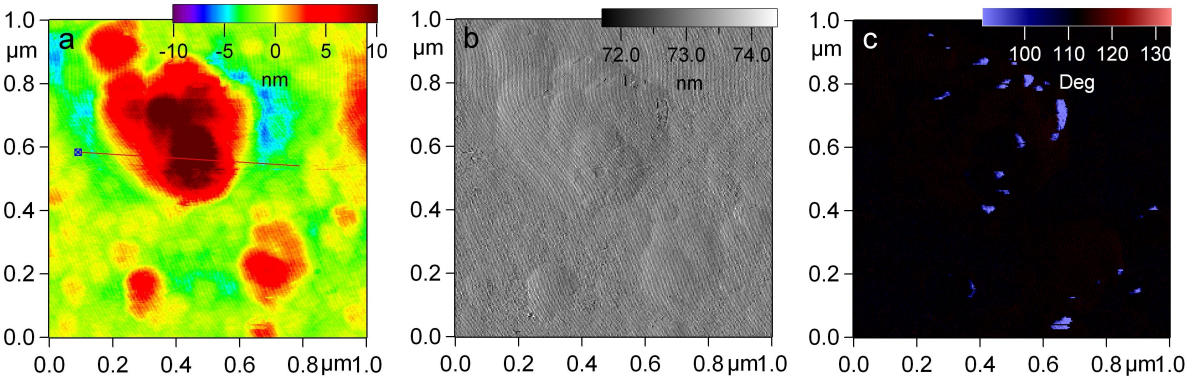

Figure 5.16: $DPPGNP^+$ with TH imaged by AFM in (a) height, (b) amplitude and (c) phase mode.

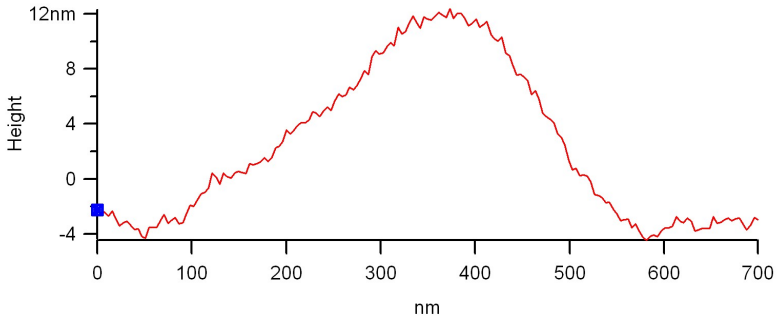

Figure 5.17: DPPGNP$^+$ with TH height profile

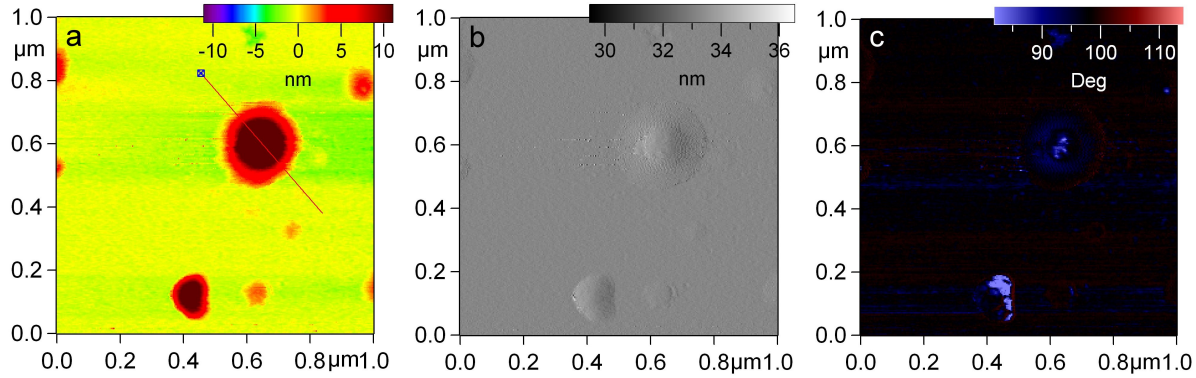

Figure 5.18: NP$^+$ loaded with TH imaged by AFM after SEC in (a) height, (b) amplitude and (c) phase mode.

nm (Figure 5.15), as it is more in accordance to the actual height. Thus, it seems that gel filtration is successful in removing some background from free TH that deposits on the mica, though another explanation could be that this image was taken at a later stage of my thesis, so that I had more experience with the settings adjustments.

For all samples, a deformation of the NPs could be observed. The NPs' sizes are expected to be 65 and 90 nm for NP$^+$ and DPPGNP$^+$, respectively, [Didier Betbeder,

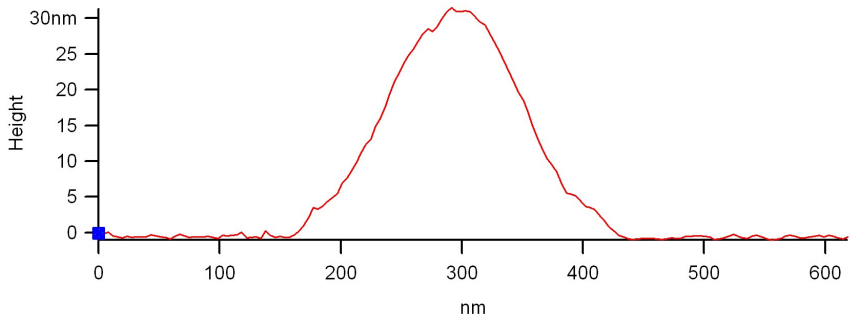

Figure 5.19: NP$^+$ with TH after SEC height profile

personal communication] and observed to be quite spherical by electron microscopy [29], but the NPs seemed always larger and thinner when imaged by AFM. The sample preparation includes drying which might force the NPs to collaps since they are porous. Another reason could be the type of tip used. The tip material might not be suitable for such soft biological samples.

5.3 TH stabilisation

As already seen in figures 5.5 and 5.7, TH activity decreases over time, and in order to test if this inactivation could be reduced we investigated the effect of several additives for TH samples both when free in solution and when bound to NPs. Gel filtration was not performed in these experiments. The initial activity of the enzyme varies from day to day due to experimental variations as exact concentration, amount of radioactively labelled L-tyrosine present in mix and the time delay between TH was thawn, but left on ice and the start of the experiment. We therefore tried to be as consequent with the conditions and accurate as possible in all experiments.

The effect of the NPs on TH activity and stability was first checked by comparing the two types of NPs to an inorganic NP made of gold and functionalised by 11-mercaptoundecanoic acid (MUA) [46], as can be seen in figure 5.20a. The NPs seem to have an intrinsic stabilising effect with NP^+ surpassing the activity level of TH alone after 1 h, whereas $DPPGNP^+$ has higher activity than TH alone only after 24 h. When data from five independent experiments are pooled, the same trends are visible and it is possible to statistically analyse the significance of the differences (Figure 5.20b). Each experiment, which always has two parallels per sample, tested at least two of the three samples displayed. The means were therefore calculated from six to ten parallels.

According to the report from a Holm-Sidak test (Appendix A.1) generated by SigmaPlot 12.0.0: '*The difference in the mean values among the different...sample*[s] *is greater than would be expected by chance after allowing for effects of differences in time. There is a statistically significant difference* ($P = 0.037$)*.*' However, when comparing the samples within one time group, the only significant difference ($P < 0.05$) was found to be at 2 min when TH-$DPPGNP^+$ was compared to TH alone or to TH-NP^+, with $P = 0.007$ and $P = 0.035$, respectively. This means that the initial decrease in activity upon binding to $DPPGNP^+$ is significant, whereas the long term stabilising effect by NP^+ or $DPPGNP^+$ are not. When NP^+ and $DPPGNP^+$ are compared to TH alone within the 24 h group, $P = 0.414$ and $P = 0.712$, respectively.

To increase the long-term activity of TH at 37°C even further, several stabilisers were

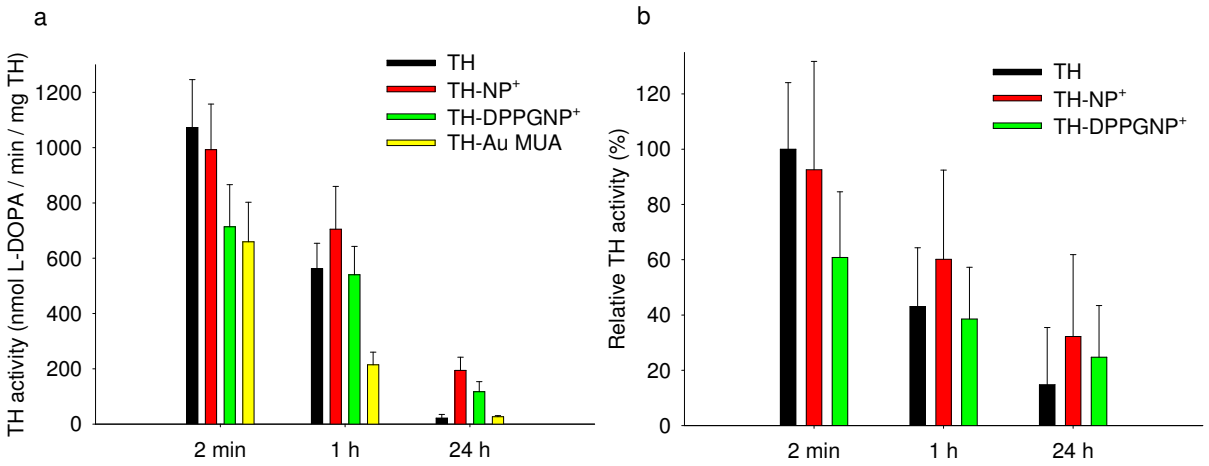

Figure 5.20: The effect of different NPs on TH activity over time and at 37°C. (a) in comparison with Au-MUA or (b) when combining five independent experiments.

tested (data not shown). Among them, BH_4 and compound III (3-amino-2-benzyl-7-nitro-4-(2-quinolyl)-1,2- dihydroisoquinolin-1-one) [47] did not increase TH activity at any time. The combination of catalase and superoxide dismutase (SOD) was however positive. Catalase and SOD are enzymes responsible for the oxidation state of the internal environment of the cell. TH requires a Fe^{2+} metal ion in its active site to be able to hydroxylase tyrosine. Since Fe^{2+} is easily oxidised to Fe^{3+}, it is important to protect Fe^{2+}. Both dopamine and compound IV also showed a stabilising effect on TH activity after 24 h. The stabilisers with the best effect on the long run were also tested in the presence of the two types of NPs (Figure 5.21).

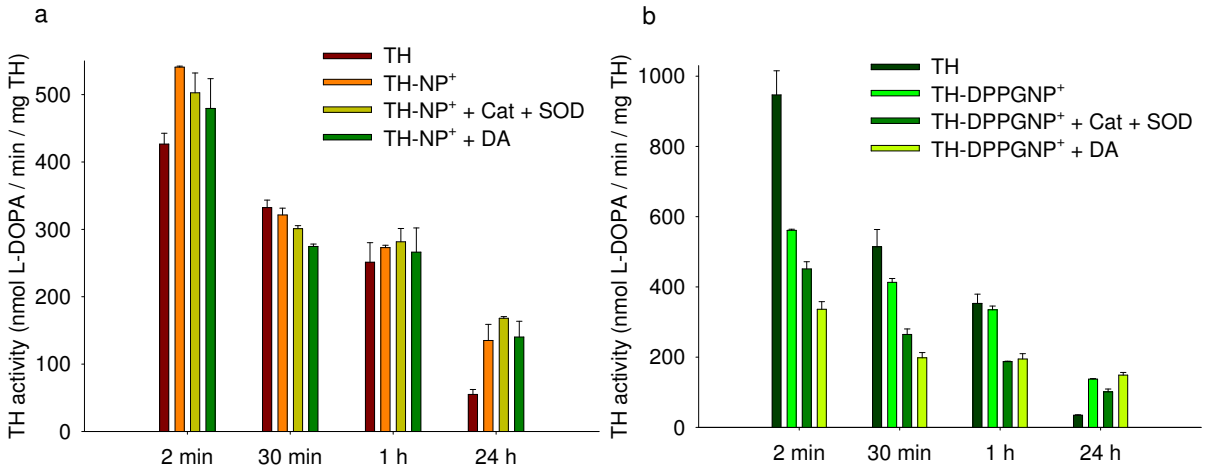

Figure 5.21: The effect of stabilisers on TH activity when (a) NP^+ or (b) $DPPGNP^+$ is present.

For NP^+ the highest activity after 24 h was obtained when Cat and SOD were present

(Figure 5.21a). When TH was bound to $DPPGNP^+$, dopamine seems the best stabiliser (Figure 5.21b).

5.4 Cell uptake of TH bound to NPs

Uptake of NP-bound TH was evaluated in four different cell types that were derived from human epithelium, rat pheochromocytoma or human embryonic kidney. The two types of epithelial cell lines, human bronchial epithelial (HBE) and human epithelial H292, were customarily used in the lab of Prof. Didier Betbeder to study the uptake of NPs bound to drugs or proteins for therapeutic delivery through the respiratory tract. Therefore we chose to use them as our model to investigate the uptake of NP-bound TH into cells.

PC12 cell line is derived from rat pheochromocytoma, which is a mild tumour of the adrenal medulla, a neuroendochrine tissue. It is a well-established cellular model for neuronal research and was selected due to its relevance to ERT for PD and related malignancies. Addition of neuronal growth factor to PC12's cell culture induces the formation of neurites, characteristic protrusions of neurons [48]. Neurites is a general term which can mean both dendrites and axons. PC12 cells intrinsically express high levels of TH, so the internal cellular environment is adapted to TH.

Human embryonic kidney cells (HEK293) were selected to serve as a model that did not contain any intrinsic TH. An up-take study was necessary for the possibility of a future evaluation of TH's functionality, to see if TH is still enzymatically active after delivery.

5.4.1 Initial testing with human epithelial cells

For cell culture experiments, purified TH protein labelled with FITC, which has a maximum emission at a wavelength of 521 nm, was used. HBE cells grown on 8-well Lab-Tek chamber slides (Thermo Scientific) were incubated for 30 min with either FITC-TH or FITC-TH bound to either NP^+ or $DPPGNP^+$. The cell nuclei were stained by 5 min incubation with DAPI, a dye with high affinity for the nucleus. Live imaging was performed using a Zeiss LSM 710 confocal microscope and 63x objective with oil immersion (Figure 5.22).

Only a few green spots, corresponding to FITC-TH, could be observed when TH alone was incubated with HBE cells (Figure 5.22a). It is possible that this TH corresponds to protein slightly associated with the outer cell membrane. When NP^+ are used for TH delivery to HBE cells (Figure 5.22b) much more TH can be seen in the cells. Large green spots indicate that TH is aggregated there, but also faint green shadows can be

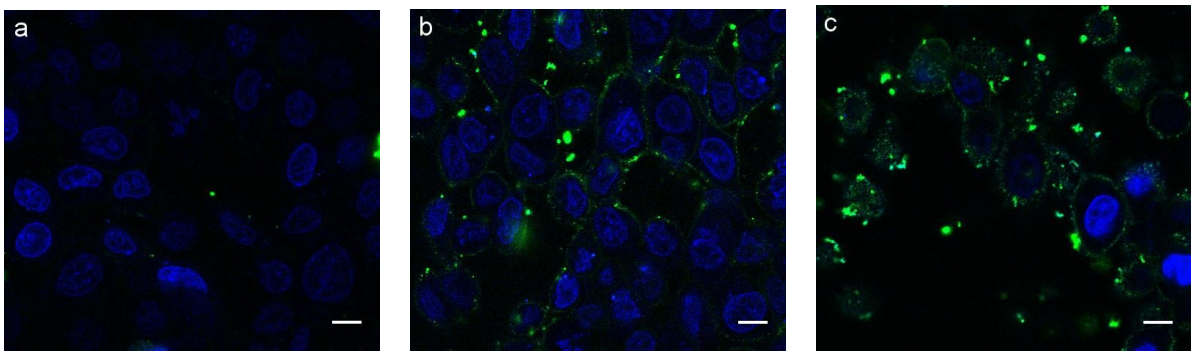

Figure 5.22: Distribution of FITC-TH (green) in living HBE cells visualised with confocal microscopy. Cell nuclei were stained with DAPI (blue). Scale bar is 10 μm. (a) TH alone, (b) TH bound to NP^+ and (c) TH bound to $DPPGNP^+$.

seen to line up which might indicate that TH bound to NP^+ is associated to the plasma membrane. When TH is delivered by $DPPGNP^+$ aggregates seem still to appear, but faint green shadows encircle the bluish labelled nuclei (Figure 5.22c). This indicates that TH is present in the cytosol.

The other human epithelial cell line, H292, grown on 8-well Lab-Tek chamber slides (Thermo Scientific), was incubated 1 h with either FITC-TH, or FITC-TH bound to either NP^+ or $DPPGNP^+$ at 37°C. The cells were fixed and then washed so that TH, that was not taken up by the cells, would be removed. Images from H292 were then taken with a Zeiss LSM 710 confocal microscope (Figure 5.23). For the H292 cells, TH seen as bright green spots, possibly from TH aggregates, dominate the images for all conditions. Only when TH is delivered by $DPPGNP^+$, some homogeneously distributed TH can be observed (Figure 5.23c).

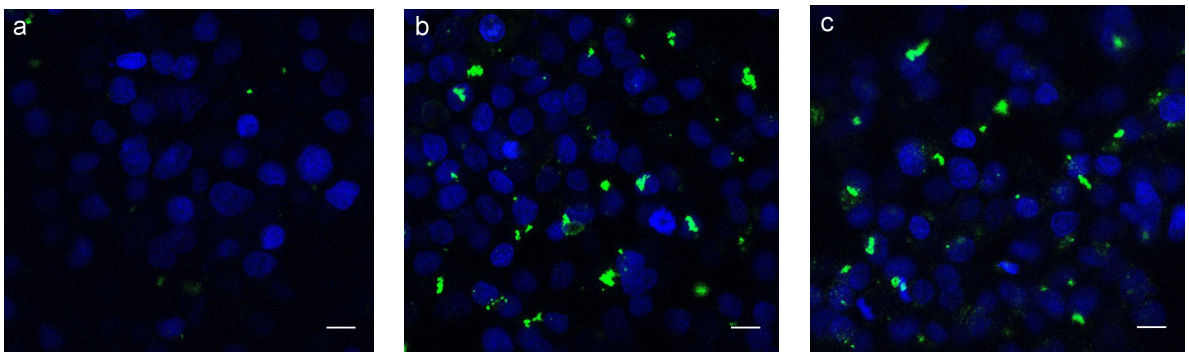

Figure 5.23: H292 cells treated with (a) FITC-TH (green) alone, (b) TH with NP^+ and (c) TH with $DPPGNP^+$. Cell nuclei are labelled with DAPI (blue). Scale bar is 10 μm.

Both human epithelial cell types seem not to have formed perfect monolayers as not all nuclei are in focus in the images. Confocal microscopes have very narrow focal planes,

so that there is a slight difference in the plane position of sample features, these rapidly goes out of focus in the image. An explanation for the absence of focus of some nuclei in the images is that nuclei are in different planes in each cell, whereas annother less plausible is that the cells have grown to form multiple layers.

5.4.2 Colocalisation of NPs and TH within epithelial cells

$DPPGNP^+$ that had been labelled with dioctadecyl tetramethylindocarbocyanine perchlorate (DiI) were used for an evaluation of the $DPPGNP^+$ position compared to TH, and to see if TH would be released after cell uptake. DiI has a maximum emission at a wavelength of 565 nm. Colocalisation of TH and $DPPGNP^+$ is shown in yellow as the superposition of red and green. HBE grown on 8-well Lab-Tek chamber slides, were imaged live after 30 min incubation with FITC-TH and DiI-$DPPGNP^+$ at 37°C and 5 min staining of the cell nuclei with DAPI (Figure 5.24).

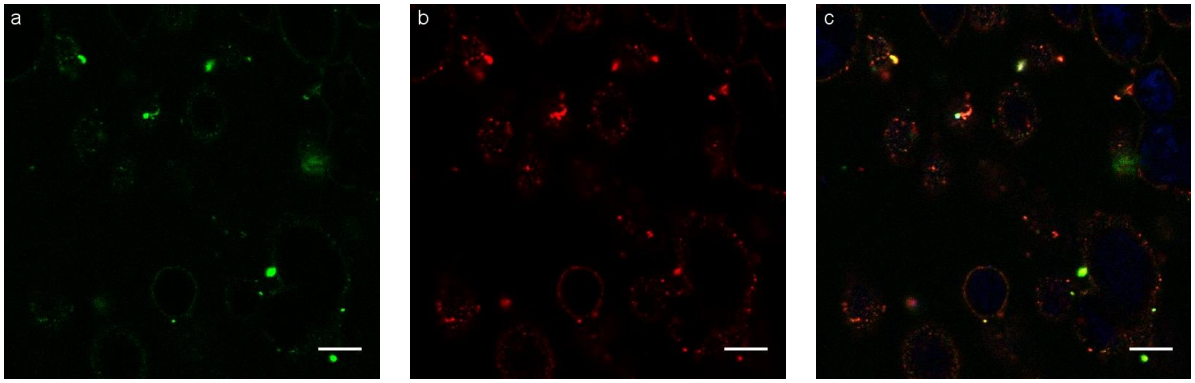

Figure 5.24: Colocalisation of FITC-TH (green) and DiI-$DPPGNP^+$ (red) in HBE cells imaged live. The colocalisation can be seen as yellow which is the superposition of red and green. Scale bar is 10 μm. (a) Green signal from FITC-TH, (b) red signal from DiI-$DPPGNP^+$ and (c) the merged image of red and green showing the colocalisation, and where the blue signal from the DAPI-stained cell nuclei can also be observed.

TH seems to bind to DiI-$DPPGNP^+$ given that the merged image from the green and red channels renders some bright yellow signals that are interpreted as colocalisation (Figure 5.24c). Nevertheless, not all NPs bind TH, given that in the merge image some red signals can be detected. Moreover, some of these are very bright probably indicating aggregated DiI-$DPPGNP^+$. Neither is all FITC-TH bound by NPs as some bright green spots can be seen in the same image. These bright green spots probably correspond to aggregated TH that is located outside the cells, which means that aggregated TH is not bound to $DPPGNP^+$ nor taken up into the cells. For the homogeneously distributed TH and NPs, it is more difficult to conclude if they colocalise or not and if TH is delivered

to the cell and then released.

Slightly different results were obtained when using the H292 cellular model (Figure 5.25). H292 cells grown on 8-well Lab-Tek chamber slides (Thermo Scientific), were incubated with FITC-TH and DiI-DPPGNP$^+$ for 1 h at 37°C. The cells were washed, fixed and stained with DAPI for 5 min and then imaged.

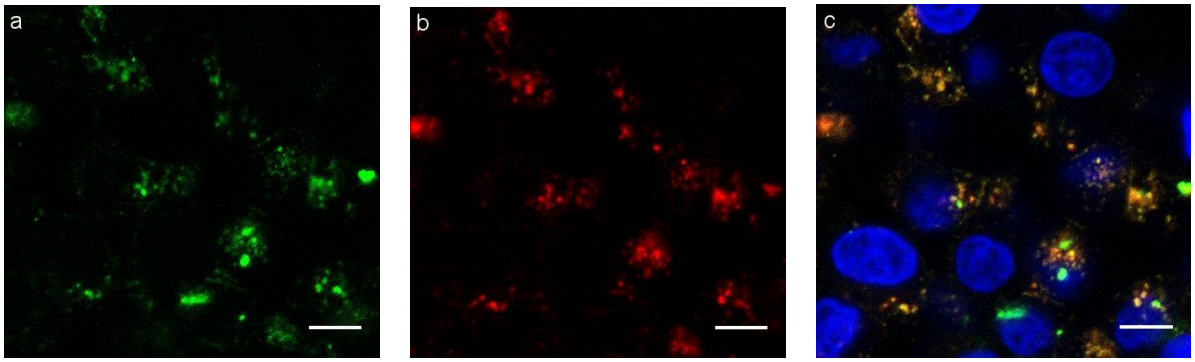

Figure 5.25: Colocalisation of FITC-TH and DiI-DPPGNP$^+$ in fixed H292 cells. Scale bar is 10 μm. (a) Green signal from FITC-TH, (b) red signal from DiD-DPPGNP$^+$ and (c) the merged image of red and green showing the colocalisation, and where the blue signal from DAPI-stained cell nuclei can also be observed.

The merged image from the FITC-TH and the DiI-DPPGNP$^+$ channels renders mainly a yellow signal (Figure 5.25c) indicating that TH binds to NP$^+$. NP$^+$ do not seem to aggregate given that no bright red spots can be observed in the merged image although some aggregated TH that is not bound the NP$^+$ is still observed as bright green spots in the merged image.

5.4.3 TH uptake into PC12 cells

For experiments to evaluate the uptake of TH to PC12 cells, TH labelled with Alexa Fluor 568, which has a maximum emission at a wavelength of 603 nm, was incubated with NP$^+$ or DPPGNP$^+$ for 10 min. Afterwards the PC12 cells, grown on coverslips coated with poly-lysine, were incubated with these mixtures or Alexa-TH alone for 1 h at 37°C. Cells were fixed and mounted using a reagent with DAPI that labels the cell nuclei. Cells were imaged with Leica TCS SP5 and images for the emission of fluorescence from Alexa and DAPI as well as bright field images were acquired. Control samples consisting of PC12 cells left untreated, showed no autofluorescence in the emission spectrum range detected (images not shown). The results of the treated PC12 cells show the same trends as for the epithelial cells. Both NPs increase the presence of Alexa-TH in the cytosol (Figure 5.26).

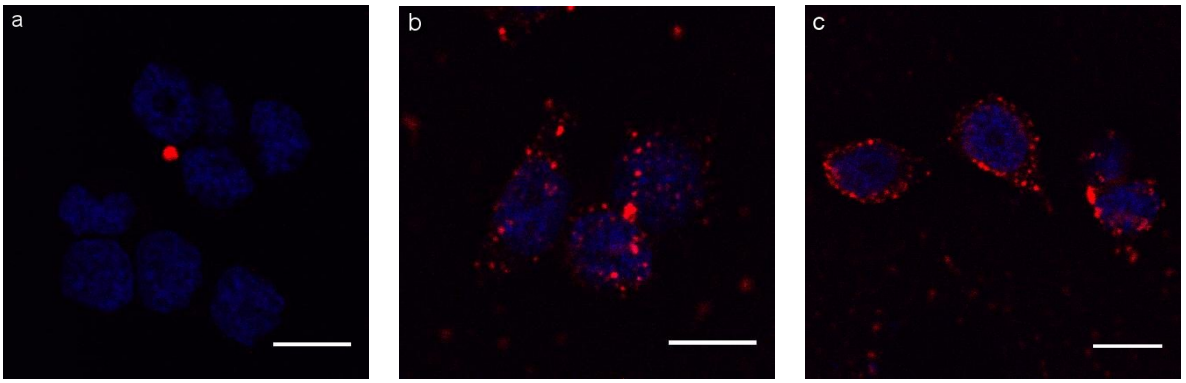

Figure 5.26: Distribution of Alexa-TH (red) in PC12 cells incubated with (a) TH alone, (b) TH with NP^+ (c) TH with $DPPGNP^+$. Cell nuclei are labelled with DAPI (blue). Scale bar is 10 μm.

It was also possible to observe PC12 cells that spontaneously had developed protrusions similar to dendrites and axons of neurons (Figure 5.27).

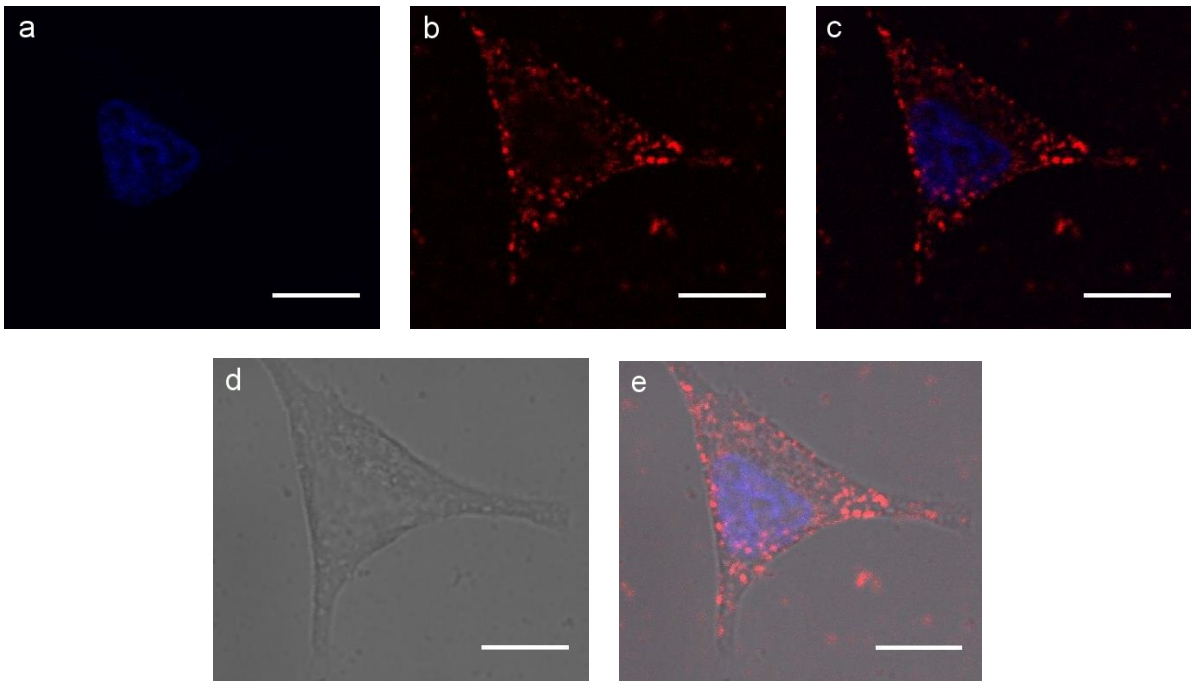

Figure 5.27: PC12 cell with neuronal morphology that has been incubated with Alexa-TH (red) bound to $DPPGNP^+$. Cell nuclei are labelled with DAPI (blue). Scale bar is 10 μm. (a) Blue signal from DAPI stained cell nucleus. (b) Red signal from Alexa-TH. (c) Superposition of blue and red signal. (d) Bright field image of PC12 cell with neuronal morphology. (e) Superposition of all signals.

Some background signal from Alexa-TH can be observed when TH is delivered by either NP^+ (Figure 5.26b) or $DPPGNP^+$ (Figure 5.26c). A possible reason for this is that the cells were seeded on poly-L-lysine coated glass coverslips to which labelled protein or the NPs might attach. We did not succeed in reducing the background even when

extensive washing with warm PBS was performed, instead of one wash with PBS at 4°C. Incubation time lapses of 1 to 3 h were carried out in order to identify the optimal incubation time for PC12 cell cultures. Nevertheless, the results did not show differences among the different incubation times (data not shown) and therefore 1 h incubation was chosen for further experiments.

5.4.4 TH uptake into HEK293 cells

HEK cells grown on coverslips coated with poly-lysine, were incubated with either Alexa-TH or Alexa-TH bound to NP^+ or $DPPGNP^+$, for 1 h at 37°C. Alexa-TH was bound to each NP by 10 min incubation at RT. HEK293 cells were fixed, counter stained and imaged using Leica TCS SP5. Images for the emission of fluorescence from Alexa and DAPI were acquired as well as bright field images. Proper controls were also carried out with HEK293 cells that were left untreated, and no signal was detected, as expected (data not shown). The images of the NP treatment of HEK293 cells show similar results as for the other cell types (Figure 5.28). A clear difference between TH uptake when TH was not delivered by any NP (Figure 5.28a) compared to when it was delivered by either NP^+ (Figure 5.28b) or $DPPGNP^+$ (Figure 5.28c) was observed. TH when delivered by any type of NP seems to cluster together in HEK293 cells, as is seen by the bright red spots.

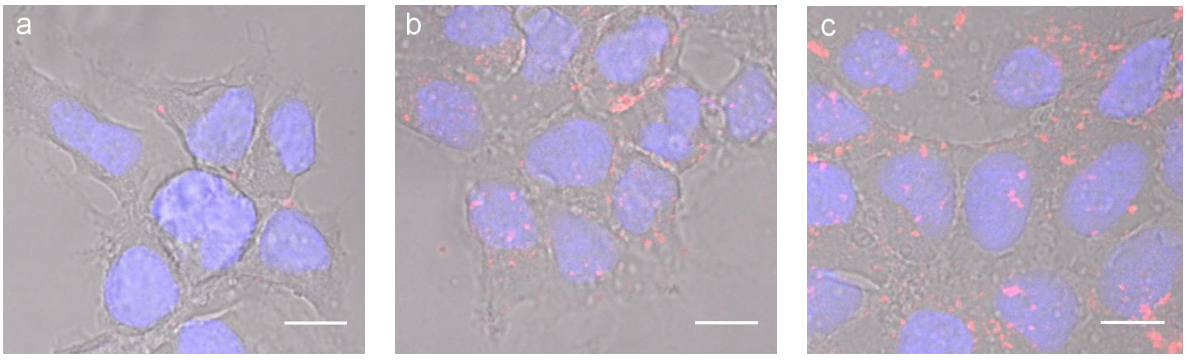

Figure 5.28: Distribution of Alexa-TH in HEK293 cells. Cell nuclei are labelled with DAPI (blue). Scale bar is 10 μm. (a) TH alone, (b) NP^+ with TH and (c) $DPPGNP^+$ with TH.

5.4.5 Penetration of TH in Z-direction

Despite the fact that all the cellular experiments and imaging described so far, indicated that TH was taken up by the cells, it is important to consider the possibility of imaging artefacts. In all cell types TH seems to be associated with the cells in some way or another when either NP^+ or $DPPGNP^+$ was present. It seems that TH must have crossed

the plasma membrane, but TH could just as well be associated to the outside of the plasma membrane or located within. To determine the exact location, z-stacks have been performed on all cell types and for both types of NPs. A z-stack is a series of images where the focus for each image is slightly moved in the Z-direction compared to the previous image and thus imaging many slices of the cell.

When TH delivery by DPPGNP$^+$s to H292 cells was imaged with the focus above most of the cell nuclei, FITC-TH appears mostly as aggregates, whereas some homogeneously distributed FITC-TH can also be observed in green (Figure 5.29a). Much more homogeneously distributed TH can be observed when the focus penetrates deeper into the cells (Figure 5.29b), whereas less TH penetrates all the way to the bottom the cells (Figure 5.29c).

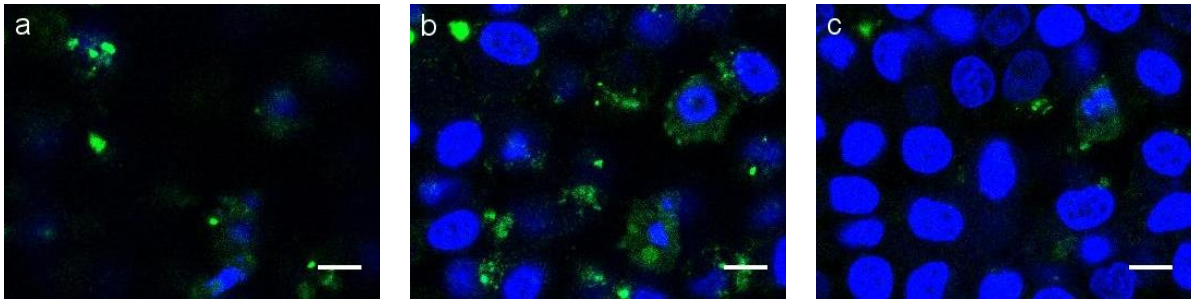

Figure 5.29: Localisation of FITC-TH delivered to H292 cells by DPPGNP$^+$ at different planes. (a) On the surface, (b) in the middle and (c) at the bottom

Slices of a PC12 cell that has developed neuronal morphology were also taken (Figure 5.30). When the focus is in the top part of the cell, some Alexa-TH can be observed where the cell is thickest (Figure 5.30a). The slice containing the middle of the nucleus shows much more TH present in the cytosol (Figure 5.30b). The bottom of the cell, much TH can be observed in the protrusions that extend along the glass coverslip (Figure 5.30c). A side view of all the z-stacks was generated by the imaging software Imaris (Bitplane) and shows the presence of TH (Figure 5.30d).

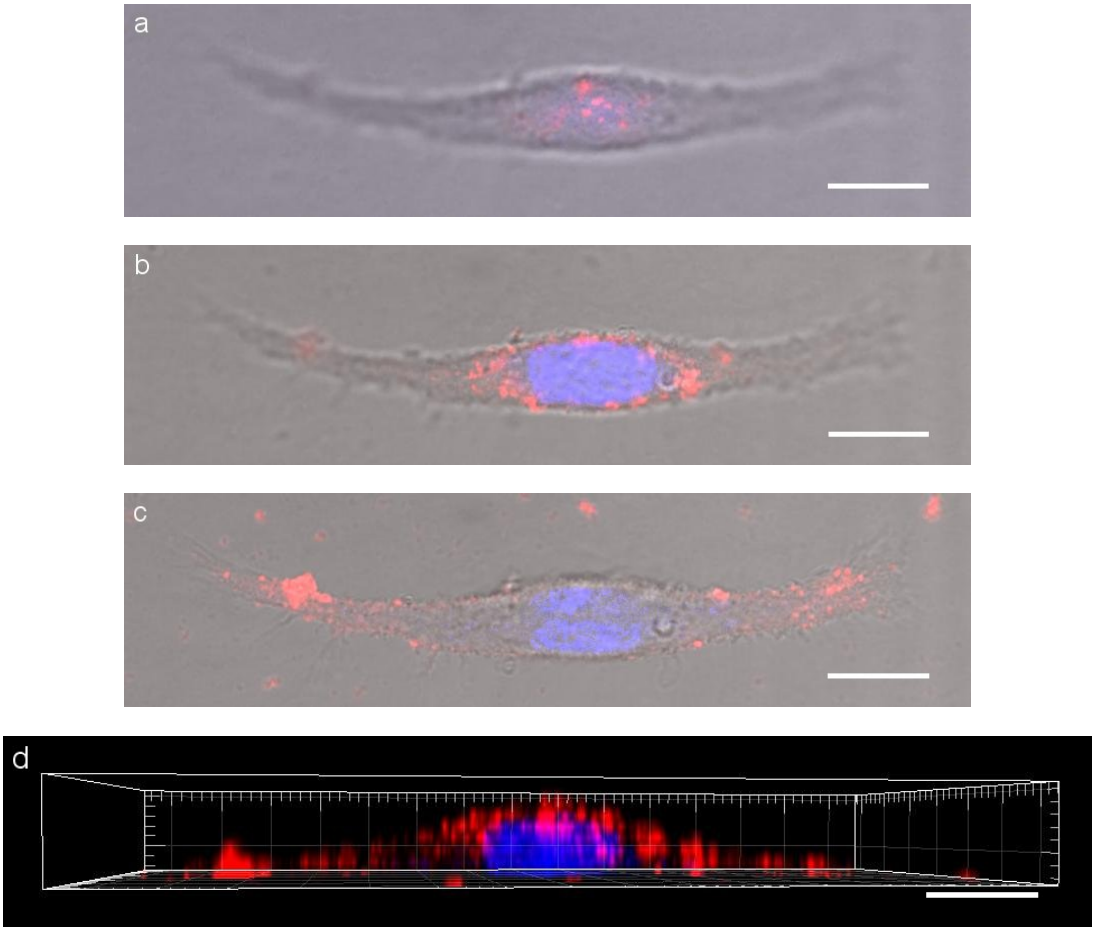

Figure 5.30: Localisation of Alexa-TH at different planes in PC12 when delivered by DPPGNP^{+}. (a) On the surface, (b) in the middle, (c) at the bottom and (d) side view of the cell.

6 Discussion

It has long been difficult to treat diseases of the brain because it is such a well protected organ. NPs as drug delivery tools have earlier been shown to be effective for the delivery of small drug and the improvement of treatments addressing brain diseases like epilepsy [49], Alzheimer's disease [50] and brain tumours [51]. The general purpose of this master's thesis has been to investigate the binding of TH to NPs and their uptake into different cell types, as a very preliminary step in the evaluation of a ERT for the treatment of dopamine deficiencies and notably PD and related malignancies. In this context, TH is the enzyme of interest because L-DOPA therapy is the standard treatment for PD. It is expected that TH delivered *in situ* would be able to increase the amount of L-DOPA in the brain when L-tyrosine, BH_4 and Fe^{2+} are naturally present. The NPs studied here have been selected according to their properties: NP^+ and for its ability of crossing the BBB [34] and $DPPGNP^+$ for its ability to avoid opsonisation [29] and for better protein delivery to cells [Didier Betbeder, personal communication].

6.1 Tyrosine hydroxylase (TH)

At the start of the project, TH was recombinantly expressed in *E. coli* as a fusion protein with MBP. A new strategy using ZZ as the fusion partner instead of MBP, was developed to improve the quality of purified TH. TH purified from the latter method, showed a higher activity after 1 h of incubation at 37°C (Figure 5.5) and a lower tendency to aggregate. Thus, the ZZ-fusion strategy appears beneficial. Optimisation by testing different *E. coli* strains and varying the induction temperature is expected to further lead to increased yield of the new expression method.

TH activity has previously been shown to be unstable, and the loss of activity over time, which has measured as a 22% loss of the initial activity after 10 min at 37°C and pH 7.0, has been explained to be caused by an inactivation rather than a denaturation of the protein [52]. The decrease in activity measured in this work, was 57% after 1 h of incubation at 37°C (Figure 5.20b). Assuming an exponential decrease of the TH activity, the predicted decrease after 10 min would be 12% which is comparable to that reported.

Part of the measured decrease of TH activity is caused by denaturation and aggregation [25]. Aggregation is a phenomenon to which all proteins are prone to in a certain

extend. Protein aggregates are toxic for human. There exist diseases like Alzheimer's and Huntington's disease where protein aggregates are the triggering factors [53]. The propensity of TH to aggregate, thought observed in vitro, has been associated to putative toxic states in vivo [25, 52]. Aggregates are especially observed when the TH batch is frequently frozen and thawn or after a dilution (data not shown). In addition, TH is not a simple protein, but a large enzyme consisting of four subunits and an easily oxidised Fe^{2+} at its catalytic site. PAH aggregation has been shown to be much more frequently happening in the iron free apo-PAH than in the holo-enzyme [24]. Temperature jumps or dilution jumps could easily induce small conformational changes which change the catalytic site and result in loss of activity. The aggregation propensity is not solely characteristic of the recombinant enzyme. In fact, when TH was purified from bovine sources, the aggregation was so severe that the standard procedure was to solubilise TH by proteolytic digestion with trypsin [54]. This gave a truncated form of TH of only 34 kDa compared to the 56 kDa per subunit of recombinant TH.

TH activity measurements indicate that there is a trend showing that both NP^+ and $DPPGNP^+$ stabilise TH, whereas the gold NPs coated with MUA show little stabilisation effects (Figure 5.20). Synthetic polymers have earlier shown to stabilise proteins by hydrophobic interactions [55]. Sugars have also been used to protect proteins from storage induced stress when proteins are integrated in NPs [56]. The use of polymeric NPs made of mainly maltodextrin might therefore aid to the conservation of TH for therapeutic use in addition to facilitate in the enzyme delivery (see below).

The enzymes that are responsible for the redox balanced environment in the cytosol, catalase and SOD, gave an additional stabilisation effect to the TH that was bound to either NP^+ or $DPPGNP^+$ (Figure 5.21). The correct oxidation state of the iron atom at the catalytically active site of TH is necessary for TH to be active. Martinez et al. showed that when the iron free apo-enzyme TH was reconsituted with Fe^{2+} an increase in stability, but no conformational change could be observed [57]. By ensuring the correct oxidation state of iron, increased stability is obtained. This might be due to prevention of Fenton's reactions induced by iron that might lead to changes around the active site and aggregation, as explained above.

In vivo, TH activity is tightly regulated by both phosphorylation and end product inhibition [22]. Phosporylation increases TH activity. A synergy between catecholamine binding to the active site and phosphorylation is also proposed as the serine 40 phosphorylation decreases the affinity for catecholamine binding [58]. TH activity is regulated by the cytosolic concentration of dopamine and other catecholamines through feed-back inhibition. The initial inhibition observed by dopamine addition to TH bound to both NP^+

and DPPGNP$^+$ (Figure 5.21) was therefore expected. Since dopamine would dissociate when the cytosolic level drops, dopamine could also stabilise TH in the long run, which was also observed for both NPs.

6.2 Nanoparticles (NPs)

The size of both types of NPs are reported to be around 60 nm in z-average diameter [29]. The sizes of the NPs batches used, are 66 nm and 85 nm for NP$^+$ and DPPGNP$^+$, respectively [Didier Betbeder, personal communication]. However, when measuring the sizes by DLS, we only reproduced the expected size for NP$^+$, whereas the size of DPPGNP$^+$ was 150 to 250 nm (Figure 5.9). The size of NP$^+$ was measured to be 53 nm in diameter which is a little smaller than reported. The reason for this difference is most probably the salt content in the buffer used. FPLC has 200 mM NaCl which is comparable to physiological salt levels, while the reported size was measured in 15 mM NaCl [29]. Since NP$^+$ is a charged particle, the water molecules will orient in such a way to cancel out the charge. The water close the the particle surface therefore forms a layer with rigid structure. DLS measures the hydrodynamic diameter which can not distinguish between the particle itself and the water shell around. The difference in the size of NP$^+$ is likely to be due to a difference in the thickness of the water shell. The more salt a solution contains, the faster it can cancel out a charge by including many counter ions in the shell of oriented water molecules.

AFM is a powerful tool with high resolution, but it is difficult to use for biological samples. When imaging metallic NPs, however, the size can easily be determined by AFM as the difference between background and particle is big as can be seen in the images of the silver NPs taken by Al-Sid-Cheikh *et al.* [59]. In all images that have been taken for this project, it has been observed that the organic NPs are deformed to a greater or lesser extend. A possible explanation is that sample preparation, which includes drying of the NPs, leads to deformation. Since the NPs are porous, it is likely that they collapse into a pancake seeming flatter and appear lower than they are in solution. AFM images of other NPs do also show a lower height than the diameter given by DLS [60, 61]. To bypass this deformation, it would be required to image in liquid with AFM, although this requires some extra expertise with the set up.

The images of NP$^+$ after free TH had been separated from bound TH gave a height of 30 nm which approaches the DLS results. Here the diameter in the AFM pictures was at least the same as given by the DLS. It has been difficult to observe any structural change to the surface and it might be that cryo-electron microscopy (cryo-EM) can help visualising

the NPs better. The NPs are then frozen down so quickly that they are expected to keep their structure. This is typically done as part of NP characterisation in addition to AFM and DLS [61].

The phase image of the AFM is not as extensively used as the height image. The structure of rubber blends has however been investigated, since the topography was not depended on the structure [62]. The phase image gives information on the interactions between the tip and the surface instead of the topography. In our study of NPs with TH there can be seen quite a change in the phase retrace images when TH is added to the NPs. The phase shift is negative (blue in figure 5.14) when TH is present instead of positive (red in figure 5.10) when TH is absent. It is likely that this change of phase is a 'signal' from TH. However, care has to be taken in these interpretations, since the phase depends on the voltage applied to the cantilever.

6.3 TH-NP conjugate

NP+ do not absorb UV light at 280 nm as is typical for proteins where this absorption arises from the presence of aromatic residues. This presents a difficulty for concentration measurements, but it is an advantage when performing SEC experiments, where the first peak in the sample with NPs and TH should therefore come from TH bound to NP^+s since the NP^+ do not give any UV signal (Figure 5.6b).

Development of ERT of mitochondrial neurogastrointestinal encephalomyopathy has been improved by incorporating the enzyme of interest, thymidine phosphorylase, into polymeric NPs [63]. No inflammatory responses were observed *in vivo* and enzyme activity decreased only a little during incubation in blood. It seems therefore plausible that further investigations into the NP-TH-conjugate could lead to a development of ERT of PD or TH deficiencies.

6.4 Uptake studies

Confocal images taken during this project, show the presence of TH (green or red depending on the labelling) in the plane of the cell nuclei of all types after 1 h of incubation with TH bound to the NPs. Evidence of NP^+ uptake in HBE cells after 3 min of incubation is reported and the fluorescence from labelled NP^+ appears to reach a plateau in these cells after 30 min [31]. The uptake might however be cell type dependent as the human epithelium is designed to attach and internalise foreign particles. The HEK293 cells did not seem to take up TH to the same extend as the PC12 or the epithelial cells. Elongated

incubation did not increase the uptake, and shorter incubation should therefore be tested. It could be that HEK293 cells take up NPs faster but also degrade or excrete them faster. This is theoretical contradictory since PC12 are cells used to secrete hormones all the time and HEK293 cells are not.

In many of the samples, big aggregates of intensely fluorescent TH at high saturation can be observed. Many of these aggregates seem to be at the cell surface as they appear in the planes where the nuclei are not at their brightest fluorescence. Since aggregates are not the TH we are interested in, and since this TH has probably not penetrated the cell membrane, the fluorescence of the aggregates can be considered an artifact. The experiment must therefore be improved to eliminate or at least diminish the formation and presence of aggregates. This can be done by a more extensive washing procedure prior to imaging. There exist numerous detergents that could improve the washing procedure and solve aggregates that have associated with the cell membrane. Some detergents like BSA, Tween or Triton could be tested and compared.

To distinguish the exact location of TH as outside but bound to the plasma membrane or in the cytosol, further experiments with plasma membrane markers have to be performed. Fluorescently labelled lipid NPs have been observed as both bound and internalised into HEK293(β3) cells using confocal microscopy and flow cytometry [64].

7 Concluding Remarks

Results from using the different methods applied in this thesis imply that TH binds to both NP^+ and $DPPGNP^+$. There is a size increase observed in the DLS, a change in the AFM phase image and an additional peak in the UV spectrum of SEC. It can therefore be proposed that TH is absorbed into the porous NPs investigated, although the specific interaction between the enzyme and the particle, a priori expected to involve the regulatory N-terminal, has not however been determined by more specific methods.

A tendency of increased TH activity after 24 h was seen when TH was incubated in the presence of either NP indicating a stabilisation effect from the NPs. Catalase and SOD or dopamine could also increase this stabilisation effect further for NP^+ and $DPPGNP^+$, respectively.

The images from the confocal microscopy analysis suggest that both NPs can deliver TH to different types of cells, whereas TH itself is not taken up by the cells.

This project has been very exciting to work with and has revealed the potential of the approach investigated to develop into a therapeutical application. In addition it has allowed to get acquainted with a number of state of the art methods, spanning from biochemistry and biophysics to cellular biology.

8 Future perspectives

An optimization of the NP to TH ratio would be an important focus for future work, since the NPs need to be positively charged in order not be opsonisated by proteins of the immune system in the blood [29]. In addition, this optimization can give information about the concentration of TH that provides maximal saturation. One approach to obtain proper titrations is to study if there is a change in the surface charge of the NPs upon binding of TH through measurements of zeta potential similar to the titration as was done for the size evaluation of the NPs as reported [65].

One of the next steps in the cell culture experiments would be to use a cell model for the BBB which can be bought commercially. This model is a kit consisting of two cell cultures: one endothelial cell line and one neuronal cell line. These cell types are grown each on its own side of a filter or membrane and serve as an artificial BBB. TH penetration across the filter from the endothelial towards the neuronal side can then be measured by concentration measurements and give an idea of the extend of BBB transcytosis.

It is not only important that TH enters physically into the brain, but also that it retains its functionality. This can be investigated by measuring TH activity of cell lysates before and after NP treatment. It has therefore been important to switch from PC12 cells to another cell line that does not have any intrinsic TH. The presence of intrinsic TH is also a disadvantage as it makes it difficult to measure the TH activity of the delivered TH as the background from the intrinsic PC12 TH will be so high. Therefore HEK293 cells were selected to serve as a model to evaluate in the near future if TH's functionality is conserved. A challenge of this planned experiment is however that if TH is not taken up into the cytosol of the cells, it might still be present in the lysate if it was associated to the plasma membrane in one or another way. Removal of TH bound to the outside of the plasma membrane has to be ensured before the measurements are performed.

At last but not at least, it is of great importance that some toxicology studies are performed on the NPs with TH. If an ERT is one day ready for patient trials, the nanocarriers should not be toxic or give any undesired effects. The study that could be performed at this moment are cell growth measurements in a controlled cell counter device which gives an indication if the NPs with TH might induce unwanted effects or even cell death.

Bibliography

[1] G. G. D'Souza and V. Weissig, "Subcellular targeting: a new frontier for drug-loaded pharmaceutical nanocarriers and the concept of the magic bullet," *Expert Opinion Drug Delivery*, vol. 6, no. 11, pp. 1135–1148, 2009.

[2] M. I. Alam, S. Beg, A. Samad, S. Baboota, K. Kohli, J. Ali, A. Ahuja, and M. Akbar, "Strategy for effective brain drug delivery," *European journal of pharmaceutical sciences : official journal of the European Federation for Pharmaceutical Sciences*, vol. 40, no. 5, pp. 385–403, 2010.

[3] S. Bhaskar, F. Tian, T. Stoeger, W. Kreyling, J. M. de la Fuente, V. Grazu, P. Borm, G. Estrada, V. Ntziachristos, and D. Razansky, "Multifunctional nanocarriers for diagnostics, drug delivery and targeted treatment across blood-brain barrier: perspectives on tracking and neuroimaging," *Particle and Fibre Toxicology*, vol. 7, no. 3, pp. 1–25, 2010.

[4] C. Celia, D. Cosco, D. Paolino, and M. Fresta, "Nanoparticulate devices for brain drug delivery," *Medicinal research reviews*, vol. 31, no. 5, pp. 716–756, 2010.

[5] P. R. Lockman, R. J. Mumper, M. A. Khan, and D. D. Allen, "Nanoparticle technology for drug delivery across the blood-brain barrier," *Drug Development and Industrial Pharmacy*, vol. 28, no. 1, pp. 1–13, 2002.

[6] S. S. Suri, H. Fenniri, and B. Singh, "Nanotechnology-based drug delivery systems," *Journal of occupational medicine and toxicology*, vol. 2, p. 16, 2007.

[7] J. Chang, Y. Jallouli, A. r. Barras, N. Dupont, and D. Betbeder, *Drug delivery to the brain using colloidal carriers*, ch. 1, pp. 1–17. 2009.

[8] G. Siegel, R. W. Albers, S. T. Brady, and D. L. Price, *Basic neurochemistry: Molecular, Cellular, and Medical Aspects*. Elsevier Academic Press, 2006.

[9] N. J. Abbott, L. Ronnback, and E. Hansson, "Astrocyte-endothelial interactions at the blood-brain barrier," *Nature reviews. Neuroscience*, vol. 7, no. 1, pp. 41–53, 2006.

[10] L. Fenart, A. Casanova, B. Dehouck, C. Duhem, S. Slupek, R. Cecchelli, and D. Betbeder, "Evaluation of effect of charge and lipid coating on ability of 60-nm nanoparticles to cross an in vitro model of the blood-brain barrier," *Journal of pharmacology and experimental therapeutics*, vol. 291, no. 3, pp. 1017–1022, 1999.

[11] U. Bickel, T. Yoshikawa, and W. M. Pardridge, "Delivery of peptides and proteins through the blood–brain barrier," *Advanced Drug Delivery Reviews*, vol. 46, p. 247–279, 2001.

[12] r. Owens, D. E. and N. A. Peppas, "Opsonization, biodistribution, and pharmacokinetics of polymeric nanoparticles," *Int J Pharm*, vol. 307, no. 1, pp. 93–102, 2006.

[13] K. S. Soppimath, T. M. Aminabhavi, A. R. Kulkarni, and W. E. Rudzinski, "Biodegradable polymeric nanoparticles as drug delivery devices," *Journal of Controlled Release*, vol. 70, pp. 1–20, 2001.

[14] R. A. Hauser, "Levodopa: past, present, and future," *European Neurology*, vol. 62, no. 1, pp. 1–8, 2009.

[15] C. W. Olanow, "Levodopa/dopamine replacement strategies in parkinson's disease–future directions," *Movement disorders : official journal of the Movement Disorder Society*, vol. 23 Suppl 3, pp. S613–22, 2008.

[16] O. Isacson and J. H. Kordower, "Future of cell and gene therapies for parkinson's disease," *Annals of Neurology*, vol. 64 Suppl 2, pp. S122–S138, 2008.

[17] A. C. Calvo, *Function and regulation of phenylalanine and tyrosine hydroxylases from human and Caenorhabditis elegans*. PhD thesis, 2010.

[18] B. Kobe, I. G. Jennings, C. M. House, B. J. Michell, K. E. Goodwill, B. D. Santarsiero, R. C. Stevens, R. G. H. Cotton, and B. E. Kemp, "Structural basis of autoregulation of phenylalanine hydroxylase," *Nature Structural Biology*, vol. 6, no. 5, pp. 442–448, 1999.

[19] K. E. Goodwill, C. Sabatier, R. Raag, P. F. Fitzpatrick, and R. C. Stevens, "Crystal structure of tyrosine hydroxylase at 2.3 Å and its implications for inherited neurodegenerative diseases," *Nature structural biology*, vol. 4, no. 7, pp. 578–585, 1997.

[20] A. H. Németh, "The genetics of primary distonias and related diseases," *Brain*, vol. 125, pp. 695–721, 2002.

[21] B. Thöny, G. Auerbach, and N. Blau, "Tetrahydrobiopterin biosynthesis, regeneration and function," *Biochemical Journal*, vol. 347, pp. 1–16, 2000.

[22] H. Fujisawa and S. Okuno, "Regulatory mechanism of tyrosine hydroxylase activity," *Biochemical and biophysical research communications*, vol. 338, no. 1, pp. 271–6, 2005.

[23] E. Olsson, K. Teigen, A. Martinez, and V. R. Jensen, "The aromatic amino acid hydroxylase mechanisma perspective from computational chemistry," vol. 62, pp. 437–500, 2010.

[24] A. Loaiza, J. A. Ronau, A. Ribbe, L. Stanciu, n. Burgner, J. W., L. N. Paul, and M. M. Abu-Omar, "Folding dynamics of phenylalanine hydroxylase depends on the enzyme's metallation state: the native metal, iron, protects against aggregate intermediates," *European biophysics journal : EBJ*, vol. 40, no. 8, pp. 959–968, 2011.

[25] F. Urano, N. Hayashi, F. Arisaka, H. Kurita, S. Murata, and H. Ichinose, "Molecular mechanism for pterin-mediated inactivation of tyrosine hydroxylase: formation of insoluble aggregates of tyrosine hydroxylase," *Journal of biochemistry*, vol. 139, no. 4, pp. 625–35, 2006.

[26] O. Lidove, M. L. West, G. Pintos-Morell, R. Reisin, K. Nicholls, L. E. Figuera, R. Parini, L. R. Carvalho, C. Kampmann, G. M. Pastores, and A. Mehta, "Effects of enzyme replacement therapy in fabry disease–a comprehensive review of the medical literature," *Genetics in medicine : official journal of the American College of Medical Genetics*, vol. 12, no. 11, pp. 668–79, 2010.

[27] J. Charrow, "Enzyme replacement therapy for gaucher disease," *Expert Opin. Biol. Ther.*, vol. 9, no. 1, pp. 121–131, 2009.

[28] M. A. Willemsen, M. M. Verbeek, E. J. Kamsteeg, J. F. de Rijk-van Andel, A. Aeby, N. Blau, A. Burlina, M. A. Donati, B. Geurtz, P. J. Grattan-Smith, M. Haeussler, G. F. Hoffmann, H. Jung, J. B. de Klerk, M. S. van der Knaap, F. Kok, V. Leuzzi, P. de Lonlay, A. Megarbane, H. Monaghan, W. O. Renier, P. Rondot, M. M. Ryan, J. Seeger, J. A. Smeitink, G. C. Steenbergen-Spanjers, E. Wassmer, B. Weschke, F. A. Wijburg, B. Wilcken, D. I. Zafeiriou, and R. A. Wevers, "Tyrosine hydroxylase deficiency: a treatable disorder of brain catecholamine biosynthesis," *Brain : a journal of neurology*, vol. 133, no. Pt 6, pp. 1810–22, 2010.

[29] A. Paillard, C. Passirani, P. Saulnier, M. Kroubi, E. Garcion, J. P. Benoit, and D. Betbeder, "Positively-charged, porous, polysaccharide nanoparticles loaded with anionic molecules behave as 'stealth' cationic nanocarriers," *Pharmaceutical Research*, vol. 27, no. 1, pp. 126–133, 2010.

[30] M. Thorolfsson, A. P. D!skeland, A. Muga, and A. Martinez, "The binding of tyrosine hydroxylase to negatively charged lipid bilayers involves the n-terminal region of the enzyme," *FEBS Letters*, vol. 519, pp. 221–226, 2002.

[31] C. Y. Dombu, M. Kroubi, R. Zibouche, R. Matran, and D. Betbeder, "Characterization of endocytosis and exocytosis of cationic nanoparticles in airway epithelium cells," *Nanotechnology*, vol. 21, no. 35, pp. 355102–355110, 2010.

[32] T. J. Kappock and J. P. Caradonna, "Pterin-dependent amino acid hydroxylases," *Chem. Rev.*, vol. 96, no. 7, pp. 2659–2756, 1996.

[33] D. Betbeder, "Mucosa administration of substances to mammals," 1998.

[34] Y. Jallouli, A. Paillard, J. Chang, E. Sevin, and D. Betbeder, "Influence of surface charge and inner composition of porous nanoparticles to cross blood-brain barrier in vitro," *International Journal of Pharmaceutics*, vol. 344, no. 1-2, pp. 103–109, 2007.

[35] M. Merhi, C. Y. Dombu, A. Brient, J. Chang, A. Platel, F. Le Curieux, D. Marzin, F. Nesslany, and D. Betbeder, "Study of serum interaction with a cationic nanoparticle: Implications for in vitro endocytosis, cytotoxicity and genotoxicity," *International Journal of Pharmaceutics*, vol. 423, no. 1, pp. 37–44, 2012.

[36] "Facilities." http://ujkeb.com/facilities.html, February 2012.

[37] N. Jalili, "A review of atomic force microscopy imaging systems: application to molecular metrology and biological sciences," *Mechatronics*, vol. 14, no. 8, pp. 907–945, 2004.

[38] http://www.chemistry.adelaide.edu.au/external/soc-rel/content/size-exc.htm, January 2012.

[39] S. W. Paddock, T. J. Fellers, and M. W. Davidson, "Basic concepts." http://www.microscopyu.com/articles/confocal/confocalintrobasics.html, February 2012.

[40] J. Bogomolovas, B. Simon, M. Sattler, and G. Stier, "Screening of fusion partners for high yield expression and purification of bioactive viscotoxins," *Protein expression and purification*, vol. 64, no. 1, pp. 16–23, 2009.

[41] B. Nilsson, T. Moks, B. Jansson, L. Abrahmsen, A. Elmblad, E. Holmgren, C. Henrichson, T. Jones, and M. Uhle, "A synthetic igg-binding domain based on staphylococcal protein," *Protein Engineering*, vol. 1, no. 2, pp. 107–113, 1987.

[42] "petzz." http://babel.ucmp.umu.se/cpep/web_content/pdf/vector%20maps/pETZZ.pdf, February 2012.

[43] F. W. Studier, "Protein production by auto-induction in high-density shaking cultures," *Protein expression and purification*, vol. 41, no. 1, pp. 207–234, 2005.

[44] J. F. Reinhard, G. K. Smith, and C. A. Nichol, "A rapid and sensitive assay for tyrosine-3-monooxygenase based upon the release of 3h2o and adsorption of [3h]-tyrosine by charcoal.," *Life sciences*, vol. 39, pp. 2185–2189, 1986.

[45] Sigma, "Blue dextran molecular weight 2,000,000 product information." http://www.chemistry.adelaide.edu.au/external/soc-rel/content/size-exc.htm, 1997.

[46] y. Halskau, S. Volden, A. C. Calvo, A. Martínez, and W. R. Glomm, "Adsorption and bioactivity of tyrosine hydroxylase on gold surfaces and nanoparticles," *Protein and Peptide Letters*, vol. 17, no. 11, pp. 1376–1382, 2010.

[47] A. C. Calvo, A. L. Pey, A. Miranda-Vizuete, A. P. Doskeland, and A. Martinez, "Divergence in enzyme regulation between caenorhabditis elegans and human tyrosine hydroxylase, the key enzyme in the synthesis of dopamine," *The Biochemical journal*, vol. 434, no. 1, pp. 133–141, 2011.

[48] L. A. Greene and A. S. Tischler, "Establishment of a noradrenergic clonal line of rat adrenal pheochromocytoma cells which respond to nerve growth factor," *Proc. Natl. Acad. Sci. USA*, vol. 73, no. 7, pp. 2424–2428, 1976.

[49] M. F. Bennewitz and W. M. Saltzma, "Nanotechnology for delivery of drugs to the brain for epilepsy," *Neurotherapeutics*, vol. 6, no. 2, p. 323–336, 2009.

[50] C. Roney, P. Kulkarni, V. Arora, P. Antich, F. Bonte, A. Wu, N. N. Mallikarjuana, S. Manohar, H. F. Liang, A. R. Kulkarni, H. W. Sung, M. Sairam, and T. M. Aminabhavi, "Targeted nanoparticles for drug delivery through the blood-brain barrier for alzheimer's disease," *Journal of controlled release : official journal of the Controlled Release Society*, vol. 108, no. 2-3, pp. 193–214, 2005.

[51] A. Beduneau, P. Saulnier, and J. P. Benoit, "Active targeting of brain tumors using nanocarriers," *Biomaterials*, vol. 28, no. 33, pp. 4947–67, 2007.

[52] B. Thony, A. C. Calvo, T. Scherer, R. M. Svebak, J. Haavik, N. Blau, and A. Martinez, "Tetrahydrobiopterin shows chaperone activity for tyrosine hydroxylase," *Journal of Neurochemistry*, vol. 106, no. 2, pp. 672–681, 2008.

[53] I. Moreno-Gonzalez and C. Soto, "Misfolded protein aggregates: mechanisms, structures and potential for disease transmission," *Seminars in cell and developmental biology*, vol. 22, no. 5, pp. 482–7, 2011.

[54] A. Vigny, M.-F. Flamand, and J.-P. Henry, "Bovine adrenal medulla tyrosine hydroxylase: Separation of the native and aggregate forms," *FEBS Letters*, vol. 86, no. 2, pp. 235–238, 1978.

[55] C. Tribet, "Hydrophobically driven attachments of synthetic po—ymers or to surfaces of biological interest: Lipid bilayers and globular proteins," *Biochimi*, vol. 80, pp. 461–473, 1998.

[56] J. Giri, W. J. Li, R. S. Tuan, and M. T. Cicerone, "Stabilization of proteins by nanoencapsulation in sugar-glass for tissue engineering and drug delivery applications," *Advanced materials*, vol. 23, no. 42, pp. 4861–7, 2011.

[57] A. Martinez, J. Haavik, T. Flatmark, J. L. R. Arrondo, and A. Muga, "Conformational properties and stability of tyrosine hydroxylase studied by infrared spectroscopy," *The Journal of Biological Chemistry*, vol. 271, no. 33, p. 19737–19742, 1996.

[58] J. Haavik, A. Martinez, and T. Flatmark, "ph-dependent release of catecholamines from tyrosine hydroxylase and the effect of phosphorylation of ser-40," *FEBS*, vol. 262, no. 2, pp. 363–365, 1990.

[59] M. Al-Sid-Cheikh, E. Pelletier, and C. Rouleau, "Synthesis and characterization of [(110m)ag]-nanoparticles with application to whole-body autoradiography of aquatic organisms," *Applied radiation and isotopes : including data, instrumentation and methods for use in agriculture, industry and medicine*, vol. 69, no. 10, pp. 1415–21, 2011.

[60] A. Cadete, L. Figueiredo, R. Lopes, C. C. Calado, A. J. Almeida, and L. M. Goncalves, "Development and characterization of a new plasmid delivery system based on chitosan-sodium deoxycholate nanoparticles," *European journal of pharmaceutical sciences : official journal of the European Federation for Pharmaceutical Sciences*, vol. 45, no. 4, pp. 451–8, 2012.

[61] J. F. Gomes, S. Rocha, M. do Carmo Pereira, I. Peres, S. Moreno, J. Toca-Herrera, and M. A. Coelho, "Lipid/particle assemblies based on maltodextrin-gum arabic core as bio-carriers," *Colloids and surfaces. B, Biointerfaces*, vol. 76, no. 2, pp. 449–55, 2010.

[62] S. Thanawan, S. Radabutra, P. Thamasirianunt, T. Amornsakchai, and K. Suchiva, "Origin of phase shift in atomic force microscopic investigation of the surface morphology of nr/nbr blend film," *Ultramicroscopy*, vol. 109, no. 2, pp. 189–192, 2009.

[63] C. De Vocht, A. Ranquin, R. Willaert, J. A. Van Ginderachter, T. Vanhaecke, V. Rogiers, W. Versees, P. Van Gelder, and J. Steyaert, "Assessment of stability, toxicity and immunogenicity of new polymeric nanoreactors for use in enzyme replacement therapy of mngie," *Journal of controlled release : official journal of the Controlled Release Society*, vol. 137, no. 3, pp. 246–254, 2009.

[64] M. Goutayer, S. Dufort, V. Josserand, A. Royere, E. Heinrich, F. Vinet, J. Bibette, J. L. Coll, and I. Texier, "Tumor targeting of functionalized lipid nanoparticles: assessment by in vivo fluorescence imaging," *European journal of pharmaceutics and biopharmaceutics : official journal of Arbeitsgemeinschaft fur Pharmazeutische Verfahrenstechnik e.V*, vol. 75, no. 2, pp. 137–147, 2010.

[65] A. V. Vergoni, G. Tosi, R. Tacchi, M. A. Vandelli, A. Bertolini, and L. Costantino, "Nanoparticles as drug delivery agents specific for cns: in vivo biodistribution," *Nanomedicine : nanotechnology, biology, and medicine*, vol. 5, no. 4, pp. 369–377, 2009.

A Appendix

A.1 Holm-Sidak test

Two Way Analysis of Variance lørdag, februar 18, 2012, 14:29:26

Data source: Rel from 5 exp ANOVA in 20120208 Comparison TH w NPs version 12

General Linear Model

Dependent Variable: Activity

Normality Test (Shapiro-Wilk) Passed (P = 0,292)

Equal Variance Test: Passed (P = 0,656)

Source of Variation	DF	SS	MS	F	P
Sample	2	4685,206	2342,603	3,452	0,037
Time	2	45734,857	22867,429	33,692	<0,001
Sample x Time	4	5565,567	1391,392	2,050	0,097
Residual	67	45473,877	678,715		
Total	75	106478,971	1419,720		

The difference in the mean values among the different levels of Sample is greater than would be expected by chance after allowing for effects of differences in Time. There is a statistically significant difference (P = 0,037). To isolate which group(s) differ from the others use a multiple comparison procedure.

The difference in the mean values among the different levels of Time is greater than would be expected by chance after allowing for effects of differences in Sample. There is a statistically significant difference (P = <0,001). To isolate which group(s) differ from the others use a multiple comparison procedure.

The effect of different levels of Sample does not depend on what level of Time is present. There is not a statistically significant interaction between Sample and Time. (P = 0,097)

Power of performed test with alpha = 0,0500: for Sample : 0,467
Power of performed test with alpha = 0,0500: for Time : 1,000
Power of performed test with alpha = 0,0500: for Sample x Time : 0,306

Least square means for Sample :

Group	Mean	SEM
TH	52,612	4,756
NP	61,650	5,318
DGNP	41,362	5,606

Least square means for Time :

Group	Mean	SEM
2 min	84,460	5,138
1 h	47,247	5,138
24 h	23,918	5,435

Least square means for Sample x Time :

Group	Mean	SEM
TH x 2 min	100,000	8,238
TH x 1 h	43,035	8,238
TH x 24 h	14,801	8,238
NP x 2 min	92,554	9,211

NP x 1 h	60,170	9,211
NP x 24 h	32,227	9,211
DGNP x 2 min	60,825	9,211
DGNP x 1 h	38,537	9,211
DGNP x 24 h	24,726	10,636

All Pairwise Multiple Comparison Procedures (Holm-Sidak method):
Overall significance level = 0,05

Comparisons for factor: **Sample**

Comparison	**Diff of Means**	**t**	**P**	**P<0,050**
NP vs. DGNP	20,288	2,626	0,032	Yes
TH vs. DGNP	11,250	1,530	0,244	No
NP vs. TH	9,038	1,267	0,210	No

Comparisons for factor: **Time**

Comparison	**Diff of Means**	**t**	**P**	**P<0,050**
2 min vs. 24 h	60,542	8,095	<0,001	Yes
2 min vs. 1 h	37,212	5,122	<0,001	Yes
1 h vs. 24 h	23,330	3,119	0,003	Yes

Comparisons for factor: **Time within TH**

Comparison	**Diff of Means**	**t**	**P**	**P<0,05**
2 min vs. 24 h	85,199	7,313	<0,001	Yes
2 min vs. 1 h	56,965	4,889	<0,001	Yes
1 h vs. 24 h	28,234	2,423	0,018	Yes

Comparisons for factor: **Time within NP**

Comparison	**Diff of Means**	**t**	**P**	**P<0,05**
2 min vs. 24 h	60,327	4,631	<0,001	Yes
2 min vs. 1 h	32,384	2,486	0,031	Yes
1 h vs. 24 h	27,943	2,145	0,036	Yes

Comparisons for factor: **Time within DGNP**

Comparison	**Diff of Means**	**t**	**P**	**P<0,05**
2 min vs. 24 h	36,099	2,566	0,037	Yes
2 min vs. 1 h	22,288	1,711	0,175	No
1 h vs. 24 h	13,811	0,982	0,330	No

Comparisons for factor: **Sample within 2 min**

Comparison	**Diff of Means**	**t**	**P**	**P<0,05**
TH vs. DGNP	39,175	3,170	0,007	Yes
NP vs. DGNP	31,729	2,436	0,035	Yes
TH vs. NP	7,446	0,603	0,549	No

Comparisons for factor: **Sample within 1 h**

Comparison	**Diff of Means**	**t**	**P**	**P<0,05**
NP vs. DGNP	21,634	1,661	0,274	No
NP vs. TH	17,135	1,387	0,311	No
TH vs. DGNP	4,498	0,364	0,717	No

Comparisons for factor: **Sample within 24 h**

Comparison	**Diff of Means**	**t**	**P**	**P<0,05**
NP vs. TH	17,426	1,410	0,414	No
DGNP vs. TH	9,925	0,738	0,712	No
NP vs. DGNP	7,501	0,533	0,596	No